



**HAL**  
open science

## **A constant influx model for dike propagation: implications for magma reservoir dynamics**

Paola Traversa, V. Pinel, J. -R. Grasso

► **To cite this version:**

Paola Traversa, V. Pinel, J. -R. Grasso. A constant influx model for dike propagation: implications for magma reservoir dynamics. *Journal of Geophysical Research: Solid Earth*, 2010, 115, pp.B01201. 10.1029/2009jb006559 . ird-00455264

**HAL Id: ird-00455264**

**<https://ird.hal.science/ird-00455264>**

Submitted on 9 Feb 2010

**HAL** is a multi-disciplinary open access archive for the deposit and dissemination of scientific research documents, whether they are published or not. The documents may come from teaching and research institutions in France or abroad, or from public or private research centers.

L'archive ouverte pluridisciplinaire **HAL**, est destinée au dépôt et à la diffusion de documents scientifiques de niveau recherche, publiés ou non, émanant des établissements d'enseignement et de recherche français ou étrangers, des laboratoires publics ou privés.

# **1 A Constant Influx Model for Dyke Propagation. 2 Implications for Magma Reservoir Dynamics**

P. Traversa,<sup>1</sup> V. Pinel,<sup>2</sup> and J.R. Grasso,<sup>1</sup>

---

J.R. Grasso, LGIT - CNRS - OSUG - Université Joseph Fourier BP 53 38041  
Grenoble Cedex 9, France.

V. Pinel, LGIT - CNRS - IRD - Université de Savoie, Campus Scientifique, 73376  
Le Bourget du Lac Cedex, France.

P. Traversa, LGIT - CNRS - OSUG - Université Joseph Fourier BP 53 38041  
Grenoble Cedex 9, France. (paola.traversa@obs.ujf-grenoble.fr)

<sup>1</sup>Laboratoire de Géophysique Interne et  
Tectonophysique, CNRS, Université Joseph  
Fourier, BP 53 38041 Grenoble Cedex 9,  
France.

<sup>2</sup>Laboratoire de Géophysique Interne et  
Tectonophysique, CNRS, IRD, Université  
de Savoie, Campus Scientifique, 73376 Le  
Bourget du Lac Cedex, France.

3 **Abstract.** Most observations of seismicity rate during dyke propagation  
4 on basaltic volcanoes show: (i) rate stationarity despite possible variations  
5 of the dyke tip velocity, (ii) frequent lack of clear and monotonic hypocen-  
6 ter migration following dyke propagation, (iii) event occurrences located back-  
7 wards with respect to the dyke tip position. On these bases, the origin of the  
8 seismicity contemporary to dyke intrusion within basaltic volcanoes cannot  
9 be solely related to the crack-tip propagation. Seismicity rather appears to  
10 be the response of the edifice itself to the volumetric deformation induced  
11 by the magma intruding the solid matrix. This in the unit time being the  
12 flux of magma entering the fracture, it argues for the stationary seismicity  
13 rate accompanying the intrusion to be a proxy for a constant magma sup-  
14 ply rate from the magma reservoir. We consider a two-phase dyke propaga-  
15 tion model, including a first vertical propagation followed by a lateral mi-  
16 gration along a lithological discontinuity. We explore (i) under which geo-  
17 physical conditions the vertical dyke is fed at constant flow rate of magma  
18 and (ii) dyke propagation patterns. Implications entailed by constant vol-  
19 umetric flux on the Piton de la Fournaise volcano case study suggest a min-  
20 imum size for the magma reservoir of about  $1 \text{ km}^3$ , and a maximum value  
21 for the initial magma reservoir overpressure of about  $2.2 \text{ MPa}$ . Considering  
22 similar magma inflow rates during vertical and lateral dyke propagation phases,  
23 we reproduce independent estimates of propagation velocities, rising times  
24 and injected volumes when applying the model to the August 2003 Piton de  
25 la Fournaise eruption.

## 1. Introduction

26 Magma-driven fracture is a commonly observed mechanism that allows  
27 to rapidly transport melt through cold and brittle country rock without  
28 extensive solidification [Lister and Kerr, 1991]. It therefore differs from  
29 porous flow through a deformable and partially molten matrix, which is  
30 characteristic of melt generation in the mantle [e.g. McKenzie, 1984] and  
31 from slow diapiric rise of granite through viscous country rock [Pitcher,  
32 1979; Rubin, 1993a].

33 The difficulty of making direct observations of the plumbing system and  
34 of the dynamics of conduit formation within volcanoes makes only approxi-  
35 mate the knowledge of the parameters and physical balances that govern the  
36 propagation of the fissure system.

37 Previous authors have proposed analytical models of fluid-driven fracture  
38 [e.g. Lister, 1990a, b; Lister and Kerr, 1991; Roper and Lister, 2005]. These  
39 studies suppose that dykes are fed from a reservoir of magma at depth;  
40 the crack is initiated within the chamber walls, where favorable conditions  
41 promote dyke propagation, leading to magmatic injections.

42 The competing pressures, whose balance drives the dyke propagation, are:  
43 (i) the elastic stresses generated by deformation of the host rock; (ii) the  
44 stresses required to extend the tip against the rock resistance; (iii) the buoy-  
45 ancy forces related to the difference between magma and country rock densi-  
46 ties; (iv) the viscous pressure drop due to magma flow; (v) the magma driv-  
47 ing overpressure; and (vi) the regional pre-existing stressfield [e.g. Lister,

48 1990b; *Lister and Kerr*, 1991]. In this framework *Lister* [1990a] concludes  
49 that the fracture mechanics only characterise the crack tip zone, while the  
50 crack width and the rate of crack propagation are determined by the fluid  
51 dynamics. Static or quasi-static solutions for equilibrium crack are therefore  
52 inappropriate. It follows that the most important role in the pressure bal-  
53 ances is played by (i), (iii), (iv) and (v). Note that (ii) is negligible "soon"  
54 away from the crack tip, and (vi) mainly acts on the dyke orientation [*Lister*,  
55 1990b; *Lister and Kerr*, 1991].

56 In the literature, dyke propagation has been modeled according to two  
57 basic independent boundary conditions. On one hand some authors consider  
58 the fluid fracture as driven by a constant overpressure magma chamber at its  
59 base [*Rubin*, 1993b, a; *Meriaux and Jaupart*, 1998; *Roper and Lister*, 2005].  
60 On the other hand *Lister* [1990a, b] assume a constant influx condition.  
61 The first hypothesis has been claimed geologically more appropriate than  
62 the second one [e.g. *Meriaux and Jaupart*, 1998]. The dyke growth model  
63 from a finite size magma chamber proposed by *Ida* [1999], however, leads the  
64 author to conclude that only in the case of extremely large and compressible  
65 magma reservoirs the melt pressure is actually able to remain constant as  
66 the dyke propagates.

67 From the observation point of view, we only have indirect access to dyke  
68 propagation, the only parameter we can estimate being the propagation ve-  
69 locity, i.e. few meters per second on basaltic volcanoes. These velocities can  
70 be deduced either from observations of the seismic signals associated with

71 the advancing crack tip [*Aki et al.*, 1977; *Shaw*, 1980; *Battaglia et al.*, 2005],  
72 or inferred from the size and composition of xenolithes carried by the flow  
73 [*Carmichael et al.*, 1977; *Spera*, 1980; *Pasteris*, 1984], or inferred from sur-  
74 face deformation measurements [e.g. *Toutain et al.*, 1992; *Battaglia and Aki*,  
75 2003; *Peltier et al.*, 2005; *Aloisi et al.*, 2006; *Peltier et al.*, 2007]. As pointed  
76 by *Battaglia et al.* [2005] and *Klein et al.* [1987], however, well-documented  
77 cases of earthquake hypocenters migrating simultaneously to the injected  
78 magma toward the surface are rare. A question mark remains on the fact  
79 that this lack of well-documented upward an monotonic earthquake migra-  
80 tion contemporary to magma ascent prior to an eruption could simply be an  
81 artefact due to a poor station coverage on many of the world's active vol-  
82 canoes [*Battaglia et al.*, 2005]. Available observations suggest however that,  
83 while vertical hypocenter migrations are uncommon, horizontal migrations  
84 appear to be more frequent (e.g. the 1978 Krafla intrusion [*Einarsson and*  
85 *Brandsdottir*, 1980], the 2000 Izu Islands magma migration [e.g. *Toda et al.*,  
86 2002]).

87 From scale-invariance explorations [*Grasso and Bachelery*, 1995] and theo-  
88 retical considerations [*Rubin and Gillard*, 1998], the distribution of recorded  
89 dyke-induced earthquakes is suggested to map the distribution of rock mass  
90 sites that are near to failure, and does not necessarily reflect the extent of  
91 the dyke. To note that only in the case of an homogeneous medium the max-  
92 imum deformation occurs at the dyke head, where we therefore expect most  
93 of the seismicity to occur [*Lister*, 1990a; *Pinel and Jaupart*, 2004]. Besides,

94 earthquakes generated from the tensile propagation of the dyke tip are likely  
95 to be too small in magnitude [*Rubin, 1995; Rubin et al., 1998*] and too high  
96 in frequency [*Cornet, 1992*] to be detected by standard seismic network that  
97 operate at volcano surface. The shear-type of the generally recorded seis-  
98 micity accompanying magma movement, moreover, is not compatible with  
99 the signal associated to a dynamic propagation of the dyke tip (i.e. a tensile  
100 fracture) [*Cornet, 1992*].

101 Observations of **Volcano-Tectonic** (VT) seismicity during dyke propagation  
102 on basaltic volcanoes show a constant seismicity rate over time [*Traversa and*  
103 *Grasso, 2009*]. This characteristic pattern for the seismic signature of dyke  
104 propagation demonstrates to be reproducible on different volcanoes: Piton  
105 de la Fournaise (PdlF): 7 dyke intrusions in the period 1988-1992; Etna:  
106 2002 dyke intrusion; and Miyakejima (MI): 2000 dyke intrusion.

107 For the Piton de la Fournaise dyke intrusions, *Traversa and Grasso* [2009]  
108 report diffuse VT seismicity within the shallow edifice. On these bases,  
109 *Traversa and Grasso* [2009] argue for the seismicity generated during dyke  
110 injection to be a generic response of the volcanic edifice to the intrusion  
111 instead of an accurate mapping of the dyke tip propagation.

112 *Toda et al.* [2002] show that the change in seismicity rate generated by  
113 the 2000 dyke intrusion at Izu Islands (Japan) scales with the change in  
114 stressing rate induced by the propagation and opening of the dyke. This re-  
115 sult demonstrates that the stressing rate governs the seismicity. It moreover

116 supports the hypothesis of magma flow rate scaling with the seismicity rate  
117 [*Pedersen et al.*, 2007].

118 All these argue for the stationary seismicity rate accompanying the dyke  
119 propagation to be the response of the brittle lithosphere to a constant volu-  
120 metric deformation rate (i.e. a constant influx of magma over time) induced  
121 by the intrusion [e.g. *Traversa and Grasso*, 2009].

122 Following *Traversa and Grasso* [2009] observations, the aim of this paper  
123 is therefore primarily (i) to analyze how a constant flow rate of magma  
124 injected into the dyke from the reservoir is consistent with the dynamics of  
125 a fluid-driven fracture propagating under realistic conditions for the magma  
126 chamber overpressure, and (ii) to evaluate the implications for the volcano  
127 dynamics. This is achieved by considering a two-phase dyke propagation  
128 model involving an initial vertical propagation phase followed by a horizontal  
129 migration phase.

130 Such two-phase propagation style for dyke propagating from a magma  
131 source at shallow depth to the surface, is commonly observed on basaltic  
132 volcanoes worldwide, e.g. Mt. Etna (southern Italy) [e.g. *Aloisi et al.*, 2006];  
133 Miyakejima (southern Japan) [e.g. *Nishimura et al.*, 2001]; and in particular  
134 on Piton de la Fournaise [e.g. *Toutain et al.*, 1992; *Bachelery*, 1999; *Peltier*  
135 *et al.*, 2005, 2007].

136 For the vertical rise of a buoyant fluid-filled crack from a shallow storage  
137 system towards the surface, we consider two boundary conditions at the  
138 dyke inlet, constant and variable reservoir overpressure. In the latter case



139 the overpressure variation is controlled by the withdrawal of magma from  
140 the chamber induced by the dyke growth. Subsequently, the effect of a  
141 lithological discontinuity at depth is introduced by reducing the buoyancy  
142 of the fluid in the upper layer. This density step induces a slow down of the  
143 rising magma and favours melt accumulation and subsequent lateral dyke  
144 propagation.

145 We apply the two-phase dyke propagation model to the magmatic intrusion  
146 that fed the August 2003 Piton de la Fournaise (PdIF) eruption. The sta-  
147 tionary rate of VT earthquakes accompanying the August 2003 PdIF dyke  
148 intrusion supports the result found by *Traversa and Grasso* [2009] in the  
149 1992-1996 period. Accordingly we expect stationary flux of magma to feed  
150 the propagating dyke. Besides, the number of works devoted to its study  
151 make it one of the best studied intrusive episodes observed on PdIF volcano  
152 in the last years.

153 This application allows us to derive possible generic implications on the  
154 mechanisms driving magma movements on basaltic volcanoes. This so-called  
155 "proximal" eruption (according to *Peltier et al.* [2008] classification) is a good  
156 example to validate our model, first as being accompanied by a stationary  
157 seismicity rate over time, and second as being constituted of a vertical- and  
158 lateral-phase dyke propagation, which is the generally accepted feature de-  
159 scribing flank eruptions at PdIF volcano [e.g. *Toutain et al.*, 1992; *Bachelery*  
160 *et al.*, 1998; *Bachelery*, 1999; *Peltier et al.*, 2005, 2007].

## 2. Models of dyke propagation

### 2.1. Vertical dyke propagation

161 In this section we **focus** on the vertical propagation of a buoyant fluid-  
 162 filled crack, from a shallow storage system towards the surface (see figure 1).  
 163 The crack is fed from a magma reservoir whose overpressure  $\Delta P_c$  is either  
 164 constant over time, or evolves as a consequence of the withdrawal of magma  
 165 from the reservoir. In particular, the aim of this section, is to individuate  
 166 whether and under which conditions, a magma reservoir is able to feed a  
 167 propagating dyke with constant flux of magma input from the reservoir.

#### 2.1.1. Model description

169 For simplicity we consider a two-layer elastic half-space, characterized by  
 170 Poisson ratio  $\nu$  and shear modulus  $G$  and subject to a lithostatic stress field.  
 171 The magma-filled fracture originates from the roof of a magma reservoir  
 172 located at depth  $H$ , which is taken as the reference level. The  $z$ -axis is  
 173 oriented positively upwards, with  $z = 0$  at the reference level, where magma  
 174 (of density  $\rho_m$ ) has developed the overpressure  $\Delta P_c$  with respect to the  
 175 surroundings. A lithological discontinuity is located at depth  $H_b$ , such that  
 176 the rock density as a function of depth is given by (see figure 1)

$$\rho_r(z) = \rho_{rl} \text{ for } z < H - H_b \text{ (lower layer),} \quad (1)$$

$$\rho_r(z) = \rho_{ru} \text{ for } z > H - H_b \text{ (upper layer).}$$

177 As demonstrated by previous authors [e.g. *Lister*, 1990a, b; *Lister and*  
 178 *Kerr*, 1991], once the dyke length is large enough, the influence of the though-

179 ness of rocks on dyke propagation can be neglected. The fluid-filled crack  
 180 propagation is in fact dominated by fluid dynamics, except during the early  
 181 nucleation of the crack, [Lister, 1990a]. On these bases, we neglect the  
 182 strength of the surrounding rocks in the force balance, and hence do not  
 183 treat stress singularity at the tip. We focus instead on the interplay between  
 184 buoyancy, viscous head loss and elastic stresses. By considering also flow-  
 185 induced stresses, the stress induced by the dyke opening is given by [Pinel  
 186 and Jaupart, 2000]:

$$\sigma_o(z) = \Delta P_c + \sigma_b(z) + p_v, \quad (2)$$

187 where  $p_v$  is the viscous head loss and  $\sigma_b(z)$  is the magma overpressure due  
 188 to buoyancy.  $\sigma_b(z)$  is given by:

$$\sigma_b(z) = \int_0^z (\rho_r(z') - \rho_m) g dz', \quad (3)$$

189 Following Pinel and Jaupart [2000] and Maaløe [1998], we fix the dyke  
 190 breadth  $a$  and we assume that the dyke adopts an elliptical cross section  
 191 with semi-axes  $a$  and  $b$  characterized by  $b(z, t) \ll a$ , see figure 1. In this  
 192 case, the dyke-induced stress is given by [Muskhelishvili, 1963]

$$\sigma_o(z, t) \approx \frac{G}{1 - \nu} \frac{b(z, t)}{a}, \quad (4)$$

193 Magma is considered as Newtonian, viscous and incompressible. Flow  
 194 proceeds in a laminar regime. According to *Pinel and Jaupart* [2000], we  
 195 obtain the following equation for the case of null lateral stress variation:

$$\frac{\partial b(z, t)}{\partial t} = -\frac{1}{4\mu} \frac{\partial}{\partial z} \left( \frac{\partial \sigma_b}{\partial z} b^3 \right) + \frac{G}{16\mu a(1-\nu)} \frac{\partial^2 b^4}{\partial z^2} \quad (5)$$

196 where  $\mu$  is magma viscosity.

197 We scale the pressures by the initial overpressure within the magma reser-  
 198 voir,  $\Delta P_c(t = 0) = \Delta P_0$ , and the front height  $z_f$  by the reservoir depth  $H$ .  
 199 Scales for time, flux and fracture width for the vertical propagation are the  
 200 following

$$[t] = \frac{16\mu H^2 G^2}{\Delta P_0^3 a^2 (1-\nu)^2}, \quad (6)$$

$$[Q] = \frac{(1-\nu)^3 \Delta P_0^4 a^4}{16G^3 \mu H}, \quad (7)$$

$$[b] = \frac{\Delta P_0 a (1-\nu)}{G}. \quad (8)$$

201 These are the reference quantities in the computation, i.e.  $[t]$  is the time-  
 202 scale for opening the crack over a length  $H$  with a uniform overpressure  $\Delta P_0$ .  
 203 Length-scale  $[b]$  is the fracture width originated by an overpressure  $\Delta P_0$ . The  
 204 scale for the dyke propagation velocity is then given by:  $[v] = H/[t]$ . The  
 205 initiation of the fracture on the reservoir walls is imposed a priori with an  
 206 elliptical profile. This affects the fracture growth only for a duration needed  
 207 for an initial adjustment stage [*Ida*, 1999]. We can define three dimensionless

208 numbers. The dimensionless number  $R_{1l}$  characterizes the magnitude of the  
 209 buoyancy force scaled to the initial overpressure, as follows

$$R_{1l} = \frac{(\rho_m - \rho_{rl})g H}{\Delta P_0} \quad (9)$$

210 Dimensionless numbers  $R_{1u}$  and  $R_2$  characterize the lithological disconti-  
 211 nuity, as follows:

$$R_{1u} = \frac{(\rho_m - \rho_{ru})g H}{\Delta P_0} \quad (10)$$

$$R_2 = \frac{H_b}{H} \quad (11)$$

212 We have therefore the following dimensionless problem to solve

$$\frac{\partial b(z, t)}{\partial t} = -4 \frac{\partial}{\partial z} \left( \frac{\partial \sigma_b}{\partial z} b^3 \right) + \frac{\partial^2 b^4}{\partial z^2}, \quad (12)$$

$$b_{(z=0, t)} = \Delta P_c(t); \quad (13)$$

213 When there is no lithological discontinuity,  $R_{1l} = R_{1u} = R_1$ , and equation  
 214 12 reduces to:

$$\frac{\partial b(z, t)}{\partial t} = 4R_1 \frac{\partial b^3}{\partial z} + \frac{\partial^2 b^4}{\partial z^2}, \quad (14)$$

215 This is solved numerically using a semi-implicit finite difference scheme  
 216 with Dirichlet boundary conditions.

217 In this framework, equation 12 allows to follow the dynamics of dyke prop-  
 218 agation on its way towards the surface. We checked that mass conservation

219 was satisfied on the scale of the whole dyke, which requires the instantaneous  
 220 volume change to be equal to the basal flux, both values being issued from  
 221 the numerical computation. The dimensions of the fracture at its base (i.e.  
 222 the imposed  $a$  value and the calculated  $b(0, t)$ , which depends on the over-  
 223 pressure at the dyke inlet) determine the volume of magma intruding into  
 224 the fissure per time unit. The velocity of the dyke propagating towards the  
 225 surface is given by  $dz_f/dt$ , where  $z_f$  is the fracture front height (see figure  
 226 1).

227 When magma is injected from the reservoir into the dyke, it induces a  
 228 decrease of the magma reservoir volume  $\Delta V_c$ , which might in turn induce a  
 229 decrease of the reservoir overpressure  $\Delta P_c$  as well. Considering the elastic  
 230 deformation induced by a point source (i.e. the magma reservoir) embedded  
 231 in an infinite medium, the evolution of the reservoir overpressure follows the  
 232 equation [V. Pinel and C. Jaupart, 2009, personal communication]:

$$d\Delta P_c(t) = \frac{dV_c(t)}{V_c(t)} \frac{4KG}{4G + 3K} \quad (15)$$

233 where  $K$  is the magma bulk modulus. The volume variation in the magma  
 234 reservoir can be related to the volume of magma injected into the dyke by

$$dV_c(t) = -Q(t)dt, \quad (16)$$

235 with  $Q$  the flux of magma entering the dyke. When magma is fully com-  
 236 pressible,  $K = 0$  and the magma reservoir overpressure remains constant  
 237 through time. For incompressible magma,  $K \rightarrow \infty$  and equation 15 becomes

$$d\Delta P_c(t) = \frac{dV_c(t)}{V_c(t)} \frac{4G}{3} \quad (17)$$

238 To fully describe the evolution of the reservoir pressure, we introduce two  
239 new dimensionless numbers:

$$R_3 = \frac{\Delta P_0 a^2 (1 - \nu) H}{G V_c}, \quad (18)$$

240 which is the inverse dimensionless reservoir volume, and

$$R_4 = \frac{4KG}{\Delta P_0 (4G + 3K)}. \quad (19)$$

241 which relates the overpressure variation in the reservoir to the initial over-  
242 pressure value.

### 243 **2.1.2. Results**

244 We study the propagation of a vertical dyke from a shallow reservoir, ac-  
245 cording to the geometry illustrated in figure 1. We investigate under which  
246 conditions the magma flux injected into the dyke **remains** constant during  
247 dyke growth. Using the dimensionless numbers above described, we discuss  
248 the role played by each parameter in determining the regime of magma flux  
249 carried by the rising dyke. We solve the problem for three different configu-  
250 rations, described here below.

251 (i) Dyke rising from a constant overpressure magma reservoir in a homoge-  
252 neous medium,

253 (ii) Dyke rising from a variable overpressure magma reservoir in a homoge-

254 neous medium,

255 (iii) Dyke rising from a variable overpressure magma reservoir in a layered  
 256 medium.

257 First we consider the case of a dyke rising from a constant overpressure  
 258 magma reservoir ( $\Delta P_c = \Delta P_0 = \text{const.}$ ) in a homogeneous medium (i.e.  
 259  $\rho_{rl} = \rho_{ru}$ ,  $R_{1l} = R_{1u} = R_1$ ). As shown in figure 2, after some numeric  
 260 adjustment iterations (whose number decreases with  $R_1$  value), the flux of  
 261 magma in the growing dyke evolves similarly to the propagation velocity  
 262 (figure 2, A and B). This is related to the fact that, in this case, the dyke  
 263 growth depends on tip propagation. Since fracture half-breadth  $a$  is assumed  
 264 constant a priori and the medium is homogeneous, the dyke only grows  
 265 along the propagation direction (figure 2, C). In this first case, the only  
 266 dimensionless number affecting the regime of magma flux over time is  $R_1$ .  
 267 We consider as negligible a flux variation less than 5% between dimensionless  
 268 dyke heights  $z_f = 0.3$  and  $z_f = 0.9$ . The choice of the first limit is imposed  
 269 by discarding initial numerical adjustment iterations. As shown in figure 3  
 270 (black open squares), the magma flux withdrawn from the reservoir **remains**  
 271 constant during dyke rising for  $R_1 \leq -3.55$ . In this constant overpressure  
 272 case, and for a given reservoir depth, the only parameter determining the  
 273 regime of the magma flux carried by the growing dyke is the ratio between  
 274 the buoyancy force and the magma overpressure at the dyke inlet.

275 Second we consider the same case as above, but with the reservoir overpres-  
 276 sure varying as magma is withdrawn. Through the dimensionless numbers



277  $R_3$  and  $R_4$ , we explore the role of the magma chamber volume  $V_c$  and of  
278 the magma bulk modulus  $K$ , which relates changes in reservoir volume with  
279 changes in pressure, on the regime of magma flux withdrawn from the reser-  
280 voir. As illustrated in figure 3 (plain symbols), the smaller the dimensionless  
281 number  $R_3$ , the more the flux tends to remain constant during dyke prop-  
282 agation and viceversa. It means that the larger the chamber volume with  
283 respect to the dyke scale volume, the more negligible a withdrawal of magma  
284 is in terms of variations in magma flow rate and reservoir overpressure dur-  
285 ing dyke rising. In the same way, the smaller the dimensionless number  $R_4$ ,  
286 the smaller the magma flux variation obtained during dyke rising and vicev-  
287 ersa. This implies that the more the magma tends to be incompressible,  
288 i.e.  $K \rightarrow \infty$ , the more the flow of magma injected into the dyke varies over  
289 time as the dyke propagates. As shown in figure 3 legend, this scenario corre-  
290 sponds to larger variations in the reservoir overpressure ( $\Delta P_c$  variation) face  
291 to the withdrawal of magma from the reservoir. Conversely, more compress-  
292 ible magmas, i.e.  $K \rightarrow 0$ , allow for smaller variations in the magma flow rate  
293 over time, which correspond to smaller overpressure variations accompany-  
294 ing magma withdrawn from the reservoir. However, only small overpressure  
295 variations ( $\Delta P_c$  variation less than  $\sim 2\%$ ) in the magma reservoir allow for  
296 the magma flow rate to remain constant during dyke propagation.

297 As a third case we consider a lithological discontinuity within the volcanic  
298 edifice. This **discontinuity** is intended in terms of rock densities, which are  
299 chosen such that magma has intermediate density between the lower and

300 upper rock layers ( $\rho_{rl} < \rho_m < \rho_{ru}$ ). This allows for considering a twofold  
 301 effect: on one hand the higher fracturation of the solid medium close to  
 302 the surface, which implies a lower density of the shallow layer and, on the  
 303 other hand, the fact that magma degasses while rising, becoming more and  
 304 more dense as approaching the surface. The effect of this density step is  
 305 to slow down the rise of magma, creating favorable conditions for magma  
 306 accumulation at the discontinuity depth  $H_b$ .

307 Figure 4 illustrates the variation of the dimensionless magma flux, propa-  
 308 gation velocity, and dyke shape during dyke propagation from an overpres-  
 309 sured magma chamber, in a two-layer medium. After an initial numeric  
 310 adjustment transient, the magma flux **remains** constant over time, being  
 311 blind to the lithological discontinuity (figure 4A). The dyke volume contin-  
 312 ues therefore to regularly grow as dyke rises. On the other hand, the dyke  
 313 propagation velocity, computed as  $dz_f/dt$ , significantly decreases when the  
 314 dyke reaches the depth of the density step (figure 4B), as also shown by  
 315 *Taisne and Jaupart* [in press, 2009].

316 Reminding that the seismic response of a volcanic edifice to dyke propaga-  
 317 tion is reported to be stationary over time [*Traversa and Grasso, 2009*], this  
 318 result supports the hypothesis of scaling between seismicity rate accompany-  
 319 ing the dyke intrusion and the volumetric flux of magma entering the dyke.  
 320 On the other hand, it excludes the possibility of a direct scaling between the  
 321 seismicity rate and the dyke propagation velocity. The density step does not  
 322 affect the shape of the fracture at the dyke inlet (figure 4C). In our model,

323 for a given magma viscosity, the magma flux supply only depends on the  
 324 shape of the crack at the junction with the reservoir roof. It can therefore  
 325 remain constant over time as dyke grows.

326 While dyke half-breadth  $a$  is assumed to be constant over time, the dimen-  
 327 sionless numbers  $R_{1rl}$ ,  $R_{1ru}$  and  $R_2$  play a role in determining the width of  
 328 the dyke at the inlet, and therefore the regime of magma flux carried by the  
 329 propagating dyke. The parameter  $R_{1rl}$  has been discussed above, while figure  
 330 5 shows the effect of  $R_{1ru}$  and  $R_2$  dimensionless numbers on the regime of  
 331 magma flow over time. In analogy with the previous discussion, we consider  
 332 as negligible a variation in the magma flux less than 5% between dimension-  
 333 less front heights  $z_f = 0.3$  and  $0.9$ . Variation in magma flux during dyke  
 334 rise are negligible for  $R_{1ru} < 1.5$  and for  $R_2 < 0.5$ . These imply that, in  
 335 order for the flux of magma to remain constant over time, the densities of  
 336 the magma and the upper layer should be quite close in value, and that the  
 337 discontinuity should not be deeper than half the reservoir depth.

338 As shown in figure 13C, when magma buoyancy faints, due to a decrease  
 339 in the surrounding rock density, an inflation starts to grow at the dyke head.  
 340 Here elastic stresses may exceed the rock toughness and new fractures may  
 341 initiate.

## 2.2. Lateral propagation at the Level of Neutral Buoyancy

342 Exhaustive description of the solution for dyke propagation at a litho-  
 343 logical boundary fed by either, constant flux or constant volume of magma  
 344 is given by *Lister* [1990b] and *Lister and Kerr* [1991]. They assume that

345 buoyancy forces do not depend on horizontal distance. The effects of lateral  
 346 variations of the stress field induced by a volcanic edifice load on the lateral  
 347 propagation are studied by *Pinel and Jaupart* [2004]. In this paper we con-  
 348 sider an horizontal lithological boundary located within the volcanic edifice.  
 349 We therefore adapt the solutions given by *Pinel and Jaupart* [2004] in order  
 350 to take into account the variation of the external lithostatic pressure induced  
 351 by the volcano slope along the propagation direction.

### 352 2.2.1. Model description

353 Figure 6 illustrates the geometry and main parameters used in this sec-  
 354 tion.  $\rho_{ru}$  and  $\rho_{rl}$  are, respectively, the rock densities in the upper and lower  
 355 layer. For this case, we define the origin of the vertical coordinate  $z$  at the  
 356 discontinuity level, oriented positive upwards. The vertical extension of the  
 357 dyke is called  $2a(x)$ .  $z_u(x)$  and  $z_l(x)$  stands for the positions of the upper  
 358 and lower dyke tips respectively, such that we have:

$$2a(x) = z_u(x) - z_l(x) \quad (20)$$

359 We also define

$$m = \frac{z_u + z_l}{z_u - z_l} \quad (21)$$

360 We neglect the effects of the free surface [*Pinel and Jaupart*, 2004], so that  
 361 the stress generated by the pressure difference between the interior and the  
 362 exterior of the dyke,  $\sigma_o$ , is given by

$$\sigma_o(x, z) = (\rho_{ru} - \rho_m)gz - \sigma_l(x) + p, \quad \text{if } z > 0 \quad (22)$$

$$\sigma_o(x, z) = (\rho_{rl} - \rho_m)gz - \sigma_l(x) + p, \quad \text{if } z < 0, \quad (23)$$

363 where  $p$  is the internal magma pressure, which varies due to viscous fric-  
 364 tion, and  $\sigma_l$  is the lithostatic pressure at the lithological boundary, defined  
 365 by:

$$\sigma_o(x) = \rho_{ru}g(H_b - \theta x), \quad (24)$$

366 with  $\theta$  the volcano slope.

367 We consider that the lateral dyke length is larger than its height and we  
 368 neglect vertical pressure gradients due to upward flow within the dyke [*Lister*  
 369 *and Kerr*, 1991; *Pinel and Jaupart*, 2004]. In this case, the internal magma  
 370 pressure  $p$  depends only on the lateral position  $x$ . As before, the condition  
 371 for the crack to remain open is  $\sigma_o > 0$ .

372 We consider that the dyke propagates in damaged rocks, and therefore we  
 373 set to zero the stress intensity factor at both dyke tips [*Mériaux et al.*, 1999].

374 Following *Pinel and Jaupart* [2004], this leads to

$$\arcsin m + m\sqrt{1 - m^2} = \frac{\pi}{2} \frac{\rho_{rl} + \rho_{ru} - 2\rho_m}{\rho_{rl} - \rho_{ru}} \quad (25)$$

$$\sigma_o(x, z = 0) = \frac{g}{\pi} (\rho_{rl} - \rho_{ru}) a(x) (1 - m^2)^{3/2} \quad (26)$$

375 It means that for given values of densities  $\rho_{ru}$ ,  $\rho_{rl}$  and  $\rho_m$ , once the over-  
 376 pressure at the lithological discontinuity is known at a given lateral distance

377  $x$ , there is a unique solution for the half-height  $a(x)$  and the tip locations  
 378  $z_u(x)$  and  $z_l(x)$ . This solution can be subsequently used to calculate the  
 379 dyke width  $b(x, z)$  using the solution derived from *Pinel and Jaupart* [2004].  
 380 For  $-1 < s < 1$ , the half-width  $b(s)$  is given by:

$$\begin{aligned}
 b(s, x) = & \frac{(1-\nu)\sigma_o(x, z=0)}{G} \sqrt{1-s^2} \\
 & + \frac{a(x)(1-\nu)g(\rho_{rl}-\rho_{ru})}{G\pi} \left[ \sqrt{1-s^2} \left( -\frac{1}{2}\sqrt{1-m^2} - \frac{1}{2}s \arcsin m - m \arcsin m \right) \right. \\
 & \quad \left. - \frac{1}{2}(s+m)^2 \ln \left| \frac{1+sm + \sqrt{(1-s^2)(1-m^2)}}{s+m} \right| \right. \\
 & \quad \left. + \frac{\rho_{ru} + \rho_{rl} - 2\rho_m}{\rho_{rl} - \rho_{ru}} \sqrt{1-s^2} \left( \frac{1}{4}s\pi + \frac{1}{2}m\pi \right) \right]
 \end{aligned} \tag{27}$$

where  $s$  is defined by:

$$s = \frac{z}{a(x)} - m.$$

381 From equation 25, we can see that dyke extension in the upper medium  
 382 is equal the extension in the lower medium ( $m = 0$ ) just in case  $\rho_{rl} - \rho_m =$   
 383  $\rho_m - \rho_{ru}$ . As there is no lateral variations of the stress field vertical gradient,  
 384  $m$  is a constant.

385 The dyke internal pressure  $\sigma_o$ , which keeps the dyke open, varies laterally  
 386 because of both, the volcano flank slope and the viscous head losses due to  
 387 horizontal magma flow. Magma is considered as Newtonian, viscous and  
 388 incompressible. Flow proceeds in laminar regime.

389 Following *Pinel and Jaupart* [2004] analytical procedure, the dyke half-  
 390 height  $a(x, t)$ , is the solution of the following equation

$$c_1 g(\rho_{ru} - \rho_m) \frac{\partial a(x,t)^3}{\partial t} = \frac{c_3(1-\nu)^2}{3\mu G^2} \frac{\partial}{\partial x} \left[ a(x,t)^7 g^3 (\rho_{ru} - \rho_m)^3 \left( \frac{g(\rho_{rl} - \rho_{ru})}{\pi} (1-m)^{3/2} \frac{\partial a(x,t)}{\partial x} - \rho_{ru} g \theta \right) \right]. \quad (28)$$

391 where

$$c_n = \int_{-1}^1 f(s)^n ds, \quad (29)$$

$$f(s) = \frac{Gb(s)}{g(1-\nu)(\rho_{ru} - \rho_m)a(x)}. \quad (30)$$

392 We scale the pressures by the lithostatic load of the rock mass above the  
393 density step,

$$[P] = \rho_{ru} g H_b. \quad (31)$$

394 the flux by the input flux of magma  $Q_{in}$  and all length dimensions by the  
395 depth of the lithostatic discontinuity  $H_b$ . The scale for the time refers to the  
396 opening of a fissure over a length  $H_b$  with a magma flux equal to  $Q_{in}$ , and  
397 is given by the following equation:

$$[t] = \left( \frac{\mu (1-\nu) H_b^9}{G Q_{in}^3} \right)^{1/4}, \quad (32)$$

398 As shown by *Pinel and Jaupart* [2004], two dimensionless numbers can be  
399 defined:

$$N_1 = \frac{3Q_{in}^{3/4} \mu^{3/4} G^{9/4}}{H_b^{9/4} (1-\nu)^{9/4} [P]^3} \quad (33)$$

$$N_2 = -\frac{2H_b^3(1-\nu)^3[P]^4}{3\mu Q_{in}G^3} \quad (34)$$

400 Equation 28 can be rewritten in the dimensionless form:

$$\frac{c_1}{c_3} N_1 \frac{\rho_{ru} - \rho_m}{\rho_{ru}} \frac{\partial a^3}{\partial t} = -\theta \frac{(\rho_{ru} - \rho_m)^3}{\rho_{ru}^3} \frac{\partial a^7}{\partial x} + \frac{(1-m)^{3/2}(\rho_{ru} - \rho_m)^3(\rho_{rl} - \rho_{ru})}{8\pi\rho_{ru}^4} \frac{\partial^2 a^8}{\partial x^2} \quad (35)$$

401 The dimensionless flux is given by:

$$\frac{q}{Q_{in}} = N_2 c_3 a(x, t)^7 \frac{(1-m)^{3/2}(\rho_{ru} - \rho_m)^3(\rho_{rl} - \rho_{ru})}{8\pi\rho_{ru}^4} \left[ \frac{\partial a(x, t)}{\partial x} - \theta \right] \quad (36)$$

402 We solve numerically this equation with a semi-implicit finite difference  
403 scheme with a Neumann boundary conditions at the source ( $x = 0$ ).

### 404 2.2.2. Results

405 In this section we discuss the effect of the model parameters on the propa-  
406 gation of a dyke at a lithological boundary, fed by a constant flux of magma.  
407 As discussed in the previous section, the dyke propagation is affected by the  
408 variation in the external lithostatic pressure induced by the volcanic slope  
409 along the propagation direction, while vertical stress gradients do not vary  
410 laterally.

411 *Lister* [1990b], discusses the case of a dyke fed by constant flux or constant  
412 volume of magma, laterally propagating in a medium with no lateral stress  
413 variations. In this case the breadth of the dyke ( $2a(x)$  in figure 6) varies in  
414 time all along its length, being however always largest at the origin ( $2a(x =$   
415  $0)$ ). *Pinel and Jaupart* [2004] consider the effect of the volcanic edifice load



416 on the propagation of a lateral dyke at depth. In this case, the breadth  
417 of the dyke varies at the head during lateral propagation, due to lateral  
418 variations of vertical stress gradients. For the present case, the lateral stress  
419 variations are only due to the flank slope of the edifice. Figure 7 shows  
420 that, with small flank slopes ( $\theta \rightarrow 0$ ), the breadth of the dyke grows at  
421 the origin as the dyke propagates, reminding the case discussed by *Lister*  
422 [1990b]. With higher flank slopes, the half-breadth  $a$  tends to a constant  
423 value as the dyke laterally propagates. Such constant value does not depend  
424 on the propagation distance from the origin. In this sense, the effect of the  
425 volcano flank slope  $\theta$  is such that it carries back to the previously discussed  
426 vertical propagation case, where the breadth  $2a$  of the dyke was assumed to  
427 be constant during propagation.

### 3. Case study: The August 22 2003, Piton de la Fournaise eruption

#### 3.1. Overview on PdIF storage and eruptive system

428 The Piton de la Fournaise (PdIF), Reunion Island, Indian Ocean, is a  
429 well-studied basaltic intraplate strato-volcano, with a supply of magma from  
430 hotspots in the mantle [see e.g. *Lénat and Bachèlery*, 1990; *Aki and Ferrazz-*  
431 *ini*, 2000; *Battaglia et al.*, 2005; *Peltier et al.*, 2005, among others]. There  
432 are five conceptual models describing the shallow storage system at PdIF vol-  
433 cano. First, *Lénat and Bachèlery* [1990] propose a model of summit reservoir  
434 composed by many small independent shallow magma pockets, located above  
435 sea level at a depth of about 0.5-1.5 km beneath Dolomieu crater. This model  
436 is supported by the cellular automaton model of *Lahaie and Grasso* [1998]

437 during the 1920-1992 period, which considers basaltic volcanoes as complex  
438 network of interacting entities at a critical state. A  $1-10 \times 10^6 \text{ m}^3$  volume  
439 has been estimated for such magma batches through spatial extent of seis-  
440 micity [*Sapin et al.*, 1996]. This range spans the volumes of lava emitted  
441 by the eruptions occurred at PdlF in the period 1972-1992 [*Sapin et al.*,  
442 1996; *Peltier et al.*, 2009], while about 32% of eruptions occurred since 1998  
443 emitted lava volumes larger than  $10 \times 10^6 \text{ m}^3$  [*Peltier et al.*, 2009].

444 Second *Sapin et al.* [1996], on crystallization arguments point out, however,  
445 that in order to produce eruptions with lava volumes of order  $1-10 \times 10^6 \text{ m}^3$ ,  
446 the volume of magma in the chamber needs to be larger than the emitted  
447 volume. They therefore suggest, as a better candidate for the Piton de  
448 la Fournaise magma reservoir, the low seismic-velocity zone identified by  
449 *Nercessian et al.* [1996] at about sea level. This aseismic zone is located just  
450 below the depth at which pre-eruptive seismic swarms are generally located,  
451 and extends at depths of 1.5-2 km below sea level. It implies a second magma  
452 chamber model volume of  $1.7-4.1 \text{ km}^3$ .

453 Third, *Albarède* [1993], by applying Fourier analysis of the Ce/Yb fluctua-  
454 tions in the Piton de la Fournaise lavas over the 1931-1986 period, estimates  
455 a magma residence time in the reservoir between 10 and 30 years. This re-  
456 sult, combined with magma production rates, lead the author to conclude  
457 that the maximum size of the PdlF magma chamber may hardly exceed 1  
458  $\text{km}^3$ .

459 Fourth *Sigmarsson et al.* [2005] uses  $^{238}\text{U}$ -series disequilibria of basalts  
460 erupted at PdIF during the period 1960-1998 to estimate magma residence  
461 time and to infer a volume of  $0.35 \text{ km}^3$  for the Piton de la Fournaise shallow  
462 magma reservoir.

463 Five, *Peltier et al.* [2007, 2008], on tilt, extensometer and GPS data ba-  
464 sis, describe the PdIF eruptions since 2003, as fed from a common magma  
465 chamber located at a depth of 2250-2350 m beneath the summit and with  
466 a radius of  $\sim 500 \text{ m}$ . This corresponds to a reservoir volume of about  $0.5$   
467  $\text{km}^3$ . The eventuality of deeper storage systems has been discussed by *Aki*  
468 *and Ferrazzini* [2000], *Battaglia et al.* [2005], *Prôno et al.* [2009] and *Peltier*  
469 *et al.* [2009]. Hence, the presence, location and size of reservoirs below Piton  
470 de la Fournaise still remain an open question.

471 As discussed in previous studies [e.g. *Toutain et al.*, 1992; *Bachelery et al.*,  
472 1998; *Peltier et al.*, 2005], flank eruptions at Piton de la Fournaise generally  
473 consist of two phases: an initial vertical rise of magma followed by a near-  
474 surface lateral migration towards the eruption site.

475 For the 2000-2003 period, *Peltier et al.* [2005] observe a correlation between  
476 the duration of the lateral propagation stage and the distance of the eruptive  
477 vents from the summit. Since the seismic crisis onset coincides with the  
478 beginning of the first propagation phase [e.g. *Peltier et al.*, 2005, 2007; *Aki*  
479 *and Ferrazzini*, 2000], *Peltier et al.* [2005] calculate a mean vertical speed  
480 of about  $2 \text{ m s}^{-1}$ , while lateral migration velocities range between 0.2 and  
481  $0.8 \text{ m s}^{-1}$ . This results are similar to those reported by *Toutain et al.* [1992]

482 for the April 1990 PdIF eruption (i.e.  $2.3 \text{ m s}^{-1}$  for the vertical propagation  
 483 and  $0.21 \text{ m s}^{-1}$  for the lateral migration) and *Bachelery et al.* [1998] for the  
 484 eruptions taking place during the first sixteen years of the PdIF Observatory  
 485 (1980-1996).

486 In this paper we focus on the August 2003 dyke intrusion, which has been  
 487 extensively studied through extensometer, tiltmeter, GPS and INSAR data  
 488 by *Peltier et al.* [2005, 2007], *Froger et al.* [2004] and *Tinard* [2007]. The dyke  
 489 intrusion is accompanied by a seismic crisis of around 400 volcano-Tectonic  
 490 (VT) events within 152 min (figure 8).

491 Seismic data illustrated in figure 8 confirm for the August 2003 case the  
 492 seismic rate stationarity observed by *Traversa and Grasso* [2009] for the PdIF  
 493 intrusions in the 1988-1992 period.

### 3.2. Relationships between magma flux regime and initial conditions for magma reservoir

494 Following the results obtained in section 2.1.2 for the vertical propagation  
 495 stage, and referring to the parameters listed in table 1, we can calculate an  
 496 upper bound for the reservoir initial overpressure and a lower bound for the  
 497 magma reservoir volume values, such that the reservoir is able to sustain a  
 498 constant influx magmatic intrusion.

499 The upper bound for the reservoir overpressure able to sustain a constant  
 500 magma flux injection, can be computed by referring to the vertical propaga-  
 501 tion stage within a homogeneous medium (i.e. we neglect the effect of the  
 502 upper layer, dimensionless number  $R_2 = 0$ ). We choose a large magma reser-

503 voir volume with fully compressible magma (i.e.  $R_3 \rightarrow 0$ ,  $R_4 \rightarrow 0$ ). The  
504 upper limit for the initial reservoir overpressure is given by the dimensionless  
505 number  $R_1$  corresponding to less than 5% variation in the magma flux during  
506 dyke growth (see figure 3, black empty squares). This is:  $R_1 < -3.55$ .

507 For parameters listed in table 1, this implies an initial reservoir overpres-  
508 sure  $\Delta P_0 < 2.2$  MPa. Such upper limit is compatible with the average  
509 overpressure at the dyke inlet estimated for the August 2003 PdIF dyke in-  
510 trusion, i.e. 1.7 MPa using InSAR data [*Tinard, 2007*] and at 1.1 MPa using  
511 GPS and tiltmeter data [*Peltier et al., 2007*]. Dyke inlet overpressure values  
512 computed using GPS data for PdIF eruptions between 2004 and 2006 also  
513 are in the range 1.1 - 2.2 MPa [*Peltier et al., 2008*].

514 Note that this value is one order smaller than commonly observed rock  
515 resistances. It may be characteristic of PdIF volcano, which endured 25 erup-  
516 tions in the period 1998-2007 [*Peltier et al., 2009*].

517 As regarding to the generic lower bound for the magma reservoir volume  
518 able to sustain a constant magma influx intrusion, we already discussed in  
519 section 2.1.2 the influence of the dimensionless numbers  $R_3$  and  $R_4$  on the flux  
520 regime of the propagating dyke. As shown in figure 9 for the vertical dyke  
521 propagation within a homogeneous medium case, a magma compressibility  
522  $K$  of about 1 GPa implies that the minimum reservoir volume required for  
523 the flux of magma to remain constant over time is  $> 1 \text{ km}^3$ . The volume  
524 of magma mobilized by the lateral injection has the effect of increasing the  
525 minimum size of the magma reservoir required in order to keep the flux

526 constant over the two-phase dyke propagation. In addition, the smaller  
527 the magma chamber volume, the smaller the  $R_1$  value necessary to keep  
528 the magma flux constant over time. For given reservoir depth, magma and  
529 rock densities, this implies smaller initial overpressures sustaining a constant  
530 influx of magma over time will be.

### 3.3. Relationship between magma volumes and reservoir overpressure conditions

531 *Traversa and Grasso* [2009] assimilate the intrusion process on basaltic vol-  
532 canoes to a strain-driven, variable-loading process, reminiscent of secondary  
533 brittle creep. In such a strain-driven process, the loading is free to vary over  
534 time. It means that the overpressure at the dyke inlet is free to vary over  
535 time.

536 Most of PdIF eruptions occurring in the last decades, however, are flank  
537 eruptions, with eruptive vents located close or within the central cone,  
538 [*Peltier et al.*, 2005, 2007, 2008]. According to the model proposed by *Peltier*  
539 *et al.* [2008] for the magma accumulations and transfers at PdIF since 2000,  
540 there is a hierarchy between the so-called 'distal' eruptions (occurring far  
541 from the summit cone), which release the reservoir overpressure, and 'prox-  
542 imal' or 'summit' eruptions (occurring close to or within the summit cone),  
543 which have negligible effect on the reservoir overpressure state. In this sense,  
544 we therefore expect most of PdIF recent eruptions to be accompanied by  
545 small variations of the magma reservoir overpressure.

546 For the August 2003 PdIF eruption, the total amount of magma withdrawn  
 547 from the reservoir (i.e. the volume of lava emitted plus the volume of the  
 548 dyke that keeps stuck at depth) has been estimated by *Peltier et al.* [2007]  
 549 and *Tinard* [2007] at  $7.2$  and  $7.8 \times 10^6 \text{ m}^3$ , respectively.

550 The model of small independent magma pockets proposed by *Lénat and*  
 551 *Bachèlery* [1990] implies a substantial emptying of the lens feeding each  
 552 individual eruption. This is consistent with large overpressure variations  
 553 accompanying the dyke intrusion. On the other hand, for the other four  
 554 conceptual models proposed for the PdIF reservoir system, i.e. reservoir  
 555 volumes of  $1.7\text{-}4.1 \text{ km}^3$  [*Nercessian et al.*, 1996; *Sapin et al.*, 1996],  $0.1\text{-}0.3$   
 556  $\text{km}^3$  [*Albarède*, 1993],  $0.35 \text{ km}^3$  [*Sigmarsson et al.*, 2005] and  $0.5 \text{ km}^3$  [*Peltier*  
 557 *et al.*, 2007, 2008], the magma volume withdrawn from the chamber during  
 558 the August 2003 eruption represents between  $\sim 0.2\%$  and  $\sim 2.5\%$  of the  
 559 reservoir volume. These values argue for very small overpressure variations  
 560 accompanying the dyke intrusion.

561 In order to test which of these configurations (i.e. large or small overpres-  
 562 sure variations) applies to the PdIF case, we calculate the minimum reservoir  
 563 size that would be required for the overpressure to vary of a defined small  
 564 percentage during dyke injection. By integrating equation 15 we obtain:

$$V_c = \frac{\Delta V_c}{\exp\left(\Delta P_{cvar} \left(\frac{4G+3K}{4GK}\right)\right) - 1}. \quad (37)$$

565 where  $\Delta V_c$  is the variation in reservoir volume,  $\Delta P_{cvar}$  is the variation  
 566 in reservoir overpressure induced by the dyke intrusion,  $G$  is the rock shear  
 567 modulus, and  $K$  is the magma bulk modulus.

568 We assume that the volume variation induced in the magma reservoir  
 569 from the August 2003 dyke growth corresponds to the estimations of the  
 570 dyke volume, i.e.  $\Delta V_c = 1 - 1.6 \times 10^6 \text{m}^3$  [Peltier et al., 2007; Tinard, 2007].  
 571 This is related to the fact that observations of seismicity rate during dyke  
 572 injection [Traversa and Grasso, 2009] do not give any information about the  
 573 flux evolution after the eruptive activity begins. We thus limit the validity of  
 574 the constant influx model only to the dyke injection, allowing that possible  
 575 larger pressure and flux variations could occur during lava flow at surface.  
 576 The estimated volume of lava erupted during the August 2003 eruption is  
 577  $6.2 \times 10^6 \text{m}^3$  [Peltier et al., 2007]. The total volume of magma withdrawn  
 578 from the chamber is therefore as large as  $7.2-7.8 \times 10^6 \text{m}^3$ .

579 We take as the initial reservoir overpressure the upper bound we calcu-  
 580 lated previously, i.e.  $\Delta P_0 = 2.2 \text{MPa}$  and we compute the reservoir volume  
 581 required for the magma overpressure variation  $\Delta P_c$  variation to be the 5%  
 582 of the initial reservoir overpressure, i.e.  $\sim 0.085 \text{MPa}$ . Equation 37 gives  
 583  $V_c = 5 - 8 \text{km}^3$  as the corresponding reservoir size.

584 When applying our model for vertical dyke propagation, computations of  
 585 overpressure variations induced in a realistic reservoir ( $V_c = 0.5 - 5 \text{km}^3$   
 586 [Nercessian et al., 1996; Sapin et al., 1996; Peltier et al., 2007, 2008]) by  
 587 a vertical dyke fed at constant flux, are showed in figure 3 legend. These



588 variations are  $< 6\%$ , for reservoir volumes between 0.5 and 5 km<sup>3</sup> and magma  
589 compressibility between 1 and 10 GPa.

### 3.4. Relationships between constant magma influx and dyke injection dynamics

590 In this section we derive the implications of the two-phase model on dyke  
591 injection dynamics and we test the model for the dyke intrusion that fed the  
592 August 2003, Piton de la Fournaise eruption.

593 The August 2003 PdIF eruption involves three eruptive fissures, the first  
594 within the summit zone (at 17h20 UTM), the second on the northern flank,  
595 at 2475 m asl (at 18h10 UTM), and the third lower on the northern flank,  
596 at about 2150 m asl (at 19h30 UTM) [Staudacher, [OVPF report](#)]. The  
597 eruptive activity of the first two fissures was negligible compared to the  
598 last one (the former stopped at the end of the first day of the eruption,  
599 while only the third fissure remained active throughout the eruption) [*Peltier*  
600 *et al.*, 2007, and Staudacher [OVPF report](#)]. As modeled by deformation  
601 data, the intrusion preceding this PdIF eruption includes a  $\sim 20$  minutes  
602 duration (from 14h55 to 15h15 UTM) vertical dyke propagation followed by  
603 a  $\sim 125$  minutes (from 15h15 to 17h20 UTM) lateral injection toward the  
604 north [*Peltier et al.*, 2007]. Although the 17h20 UTM time corresponds to  
605 the opening of the first summit fracture [Staudacher [OVPF report](#)], tilt data  
606 clearly indicate that the lateral dyke has already fully propagated to the flank  
607 eruption site by this time. Indeed, no further evolution of the deformation  
608 is observed after 17h20 UTM [*Peltier et al.*, 2007].

609 By inverting deformation data, *Peltier et al.* [2007] estimate the origin  
 610 of the August 2003 dyke at  $400 \pm 100$  meters asl, and the origin point of  
 611 the lateral dyke at  $1500 \pm 350$  m asl. The lateral dyke travels  $2.4 \pm 0.1$   
 612 km before breaching the surface [*Peltier et al.*, 2007]. On deformation data  
 613 basis, *Peltier et al.* [2007] estimate an average velocity of  $1.3 \text{ m s}^{-1}$  for the  
 614 vertical rising stage, and of  $0.2 - 0.6 \text{ m s}^{-1}$  for the lateral injection phase.  
 615 The uncertainties related to vertical and horizontal propagation velocities,  
 616 obtained from deformation data inversion, are  $0.26 \text{ m s}^{-1}$  and  $0.13 \text{ m s}^{-1}$ ,  
 617 respectively [uncertainties from A. Peltier 2009, personal communication].

618 In the following we calibrate the input parameters for the two-stage dyke  
 619 propagation model. First we derive the relationships among the parameters  
 620 at stake for the two steps. Second we obtain calibrations of the same pa-  
 621 rameters by using independent estimates of dyke propagation velocities in the  
 622 two phases.

623 We consider a dyke rising vertically within a homogeneous medium (i.e.  
 624  $R_2 = 0$ ), from a large magma reservoir with fully compressible magma (i.e.  
 625  $R_3 \rightarrow 0$ ,  $R_4 \rightarrow 0$ ). Reservoir depth  $H$ , magma and rock densities  $\rho_m$ ,  $\rho_r$   
 626 are listed in table 1. **In this case, the flux of magma injected into the dyke**  
 627 **only depends on the initial overpressure at the dyke inlet** and is inversely  
 628 proportional to the magma viscosity, as shown in figure 10:

$$Q \propto \frac{1}{\mu}, \quad (38)$$

629 When we fix the vertical velocity and we let the dyke half-breadth  $a$  free  
 630 to vary, however, we can write:

$$Q = A\mu, \quad (39)$$

631 where

$$A = \frac{v_v^2 Q^* 16H G}{v_v^{*2} \Delta P_0^2 (1 - \nu)} \quad (40)$$

632  $v_v$  is the vertical propagation velocity,  $Q^*$  is the dimensionless flux of  
 633 magma entering into the dyke (i.e.  $Q/[Q]$ ) and  $v_v^*$  is the dimensionless ver-  
 634 tical propagation velocity (i.e.  $v_v/[v]$ ). The vertical propagation velocity, in  
 635 turn, is given by

$$v_v = C \frac{a^2}{\mu}. \quad (41)$$

636 where

$$C = \frac{v_v^* (1 - \nu)^2 \Delta P_0^3}{16 H G^2}. \quad (42)$$

637 For a given dimensionless number  $R_1$ , the dimensionless flux and velocity  
 638 (i.e.  $Q^*$  and  $v_v^*$ ) are fixed. Then, for given values of vertical propagation  
 639 velocity, depth of the reservoir, and initial magma overpressure, we obtain  
 640 the  $A$  value.

641 We take  $R_1 = -3.55$  (i.e. the upper limit for a 5% flux variation in  
642 the constant reservoir overpressure, homogeneous medium case as shown in  
643 figure 3) and the parameters listed in table 1.

644 The lateral propagation velocity depends on the magma viscosity and on  
645 the amount of magma injected into the dyke in the unit time. We then in-  
646 ject different magma flux and viscosity pairs into the lateral dyke. Figure 11  
647 shows how the magma flux injected in the dyke is related to the lateral prop-  
648 agation velocity. In particular, a dyke lateral propagation velocity between  
649 0.2 and 0.6 m s<sup>-1</sup> (shadow box in figure 11), requires the magma flow rate  
650 injected into the laterally migrating dyke to be less than about 60 m<sup>3</sup> s<sup>-1</sup>.  
651 Through equation 39 this implies a magma viscosity  $\mu = 14$  Pa s. This allows  
652 to constrain the value of the vertical dyke half-breadth  $a = 100$  m (equation  
653 41).

654 The value we estimate for viscosity is in good agreement with the values  
655 found by *Villeneuve et al.* [2008] for remolten basalts from the 1998 lava  
656 flow of the Piton Kapur, on the northern part of Dolomieu crater. Viscosity  
657 measurement experiments conducted at constant stress indicate (i) liquidus  
658 temperature of the 1998 sample at about 1200°C and (ii) viscosities between  
659 49 and 5 Pa s measured at temperatures between 1195°C (glass transition)  
660 and 1386°C (superliquidus), respectively.

661 For the case of a dyke propagating within a stratified medium from a  
662 finite size, compressible magma chamber, more parameters play a role in  
663 characterizing the dyke propagation, i.e. magma bulk modulus  $K$ , magma

664 chamber volume  $V_c$ , rock densities in the upper  $\rho_u$  and lower  $\rho_l$  layers and  
665 the depth of the lithological discontinuity  $H_b$ . We refer to the geometry  
666 illustrated in figure 12, and we use the parameters listed in table 2 in the  
667 calculations. Table 3 compares results issued from the computation with  
668 independent parameter estimates.

669 From the computation we obtain a dyke which rises vertically at an average  
670 velocity of  $\sim 1.2 \text{ m s}^{-1}$  up to the lithological discontinuity. Figure 13 shows  
671 the effect of the density barrier on the propagation of the vertical dyke. It  
672 quantifies injected magma flux and volume and dyke vertical propagation  
673 velocity over time (figure 13A, B, C). The shape of the vertical dyke for  
674 different propagation steps is illustrated in figure 13, D. The flow of magma  
675 injected into the vertical dyke over time is  $\sim 35 \text{ m}^3 \text{ s}^{-1}$ , through a fracture  
676 of width  $b \sim 30 \text{ cm}$ , which matches with the value found by *Peltier et al.*  
677 [2007], *Froger et al.* [2004] and field observations [*Peltier et al.*, 2007].

678 The dyke extends above the discontinuity, but its upward propagation  
679 is set back by the negative buoyancy [*Pinel and Jaupart*, 2004]. At the  
680 density step depth, magma overpressure grows as the dyke head inflates. It  
681 may eventually exceed rock toughness and a new fracture may propagate  
682 laterally away. Here we set up a lateral dyke, which propagates towards the  
683 northern flank. We assume all the magma flux rising through the vertical  
684 dyke is injected into the lateral one. The slope of the edifice and the lack  
685 of lateral variation in stress gradients, allow for the dyke half-breath  $a$  to be  
686 constant during the lateral propagation (see figure 7).

687 The computed lateral dyke breadth  $2a$  is  $\sim 950$  m. The upper bound of the  
688 fracture breaches the surface at a height of about 2000 m asl after 2.3 km  
689 lateral propagation, in agreement with field observations of eruptive fracture  
690 location [*Peltier et al.*, 2007; *Tinard*, 2007]. The average propagation velocity  
691 we compute for the lateral dyke is  $\sim 0.48$  m s<sup>-1</sup>, in agreement with the upper  
692 limit value estimated by *Peltier et al.* [2007] by deformation data inversion  
693 (0.2 to 0.6 m s<sup>-1</sup>).

694 We remind that the flux of magma injected in the vertical and lateral dykes  
695 is related to the respective initial dyke breadth. From the computation we  
696 get lateral dyke breath ( $a = 476$  m) about five times the vertical dyke one  
697 ( $a = 100$  m). This is related to the fact that horizontal velocity is much  
698 lower than the vertical, which has the effect of making the dyke growing less  
699 along the propagation direction and to develop crosswise. The propagation  
700 velocity ratio, therefore, somehow inversely mimics the dyke breath ratio  
701 between the vertical and the lateral phases.

#### 4. Conclusions

702 Seismic observations contemporary to dyke propagation on basaltic vol-  
703 canoes show stationary seismicity rate during dyke propagation in the last  
704 phase before an eruption, despite possible variations of the dyke-tip velocity  
705 [*Traversa and Grasso*, 2009]. Also, a clear and monotonic hypocenter mi-  
706 gration of the seismicity contemporary to dyke propagation has been rarely  
707 observed. These suggest that the observed dyke-induced seismicity is the re-  
708 sponse of the edifice to the volumetric deformation induced by the magma in-

709 truding the solid matrix [*Traversa and Grasso, 2009*]. Accordingly, *Traversa*  
710 *and Grasso* [2009] argue for the stationary seismicity rate contemporary to  
711 the intrusion to be a proxy for a constant flux of magma entering the dyke  
712 in the unit time.

713 In order to test the implications of this assertion with respect to the vol-  
714 cano fluid dynamics, we implement a two-phase dyke propagation model,  
715 including a first vertical propagation followed by a lateral migration.

716 We demonstrate that, although propagation velocity varies of one order of  
717 magnitude among the different propagation phases (i.e.  $1.3 \text{ m s}^{-1}$  and  $0.2$  to  
718  $0.6 \text{ m s}^{-1}$  for the vertical and lateral propagation, respectively), the flow rate  
719 of magma injected into the dyke can remain constant over time under given  
720 conditions. This is related both, to the fact that velocity depend on dyke  
721 size for the two propagation phases, and to the evolution of dyke growth,  
722 which is not limited only to elongation. It supports the idea of direct scaling  
723 between the magma flux intruding the solid and the observed seismicity rate  
724 through volumetric deformation. On the other hand it rejects a direct scal-  
725 ing between the seismicity rate and the dyke propagation velocity. In this  
726 sense the seismicity rate recorded at low-viscosity volcanoes during dyke in-  
727 trusion represents the response of the solid matrix to a stationary volumetric  
728 deformation induced by the intrusion itself.

729 Obeying the laws governing fluid dynamics, the constant magma flux can  
730 be sustained by either, a constant or a slightly variable overpressure at the  
731 base of the dyke. The model we propose, however, does not allow for assert-

ing one hypothesis with respect to the other. Indeed it allows to investigate  
the implications of such a stationary flux hypothesis. For the vertical propa-  
gation, once the geometry and the physical parameters are fixed, the constant  
influx assumption bounds the range of possible initial magma overpressures  
and volumes of the magma reservoir. Specifically, only a magma reservoir  
with sufficiently small initial overpressure and sufficiently large volume is  
able to sustain a dyke injection fed at constant flux.

The flux value computed in the vertical phase is injected in the lateral propa-  
gation **phase** and it determines, together with static conditions of pressure  
equilibrium, dyke size and lateral propagation rate. In this way, the model  
we discuss in this paper allows to constrain the ratio between vertical and  
horizontal dyke thickness.

We validate the model in an application to the August 2003, Piton de  
la Fournaise eruption. It consists of two main phases: a vertical propaga-  
tion, followed by a horizontal migration towards the eruption site [*Lénat and*  
*Bachèlery, 1990; Toutain et al., 1992; Bachèlery et al., 1998; Bachèlery, 1999;*  
*Peltier et al., 2005, 2007, 2008*]. According to the classification proposed by  
*Peltier et al. [2008]*, the August 2003 PdIF eruption is a so-called 'proximal'  
eruption, with eruptive activity concentrated on the volcano flank, close to  
the central cone.

In this framework, the small values of initial reservoir overpressure (i.e.  $\leq$   
**2.2 MPa**), and the small variations of this overpressure accompanying dyke  
propagation (i.e.  $\leq 6\%$ ) we obtain from the computation, argue for this



755 eruption to belong to an early stage of a PdIF refilling cycle [see *Peltier*  
756 *et al.*, 2008]. The small overpressure variations argue for either, the volume  
757 of magma withdrawn from the reservoir during the injection to be small  
758 compared to the reservoir volume, or the magma flow rate injected into the  
759 dyke in the unit time to be small compared to a possible continuous magma  
760 flow refilling the shallow reservoir from depth (as proposed by *Peltier et al.*  
761 [2007]).

762 The average intrusion velocities we compute for the dykes feeding the  
763 August 2003 PdIF eruption well reproduce the values estimated by *Peltier*  
764 *et al.* [2007] on deformation data basis. It further support the validity of our  
765 model.

766 In conclusion, the dyke propagation model we propose, allows for validat-  
767 ing the constant magma influx initial condition as geophysically realist for  
768 volcano processes.

769 **Acknowledgments.** We thank B. Taisne and A. Peltier, for suggestions  
770 and interesting discussions. We aknowledge two anonymous reviewers for  
771 the care devoted to the review and the interesting and constructive remarks  
772 made. The data used in this study have been acquired by the Piton de la  
773 Fournaise Volcanological Observatory (OVPF/IPGP). Special thanks to V.  
774 Ferrazzini, in charge of the OVPF seismological network. P.T. and J.R.G.  
775 are supported by VOLUME-FP6 and TRIGS projects, contracts n. 08471  
776 and 043386, respectively.

## References

- 777 Aki, K., and V. Ferrazzini (2000), Seismic monitoring and modeling of an  
 778 active volcano for prediction, *J. Geophys. Res.*, *105*(B7), 16,617–16,640.
- 779 Aki, K., M. Fehler, and S. Das (1977), Source mechanism of volcanic tremor:  
 780 fluid-driven crack models and their application to the 1963 Kilauea erup-  
 781 tion, *J. Volcanol. Geotherm. Res.*, *2*, 259–287.
- 782 Albarède, F. (1993), Residence time analysis of geochemical fluctuations in  
 783 volcanic series, *Geochim. Cosmochim. Acta*, *57*(3), 615–621.
- 784 Aloisi, M., A. Bonaccorso, and S. Gambino (2006), Imaging compos-  
 785 ite dike propagation (Etna, 2002 case), *J. Geophys. Res.*, *111*(B06404),  
 786 doi:10.1029/2005JB003908.
- 787 Bachélery, P. (1999), Le Fonctionnement des volcans boucliers, Habilitation  
 788 à Diriger des Recherches thesis, Univ. de la Reunion, Saint Denis, France,  
 789 698 pages.
- 790 Bachélery, P., P. Kowalski, P. Catherine, J. Delmond, P. Blum, and J. Croce  
 791 (1998), *Precise Temporal and Mechanical Identification of Dyke Emplace-*  
 792 *ment using Deformation Monitoring at Piton de la Fournaise.*, pp. 475 –  
 793 485, European Commission, EUR 18161 EN.
- 794 Battaglia, J., and K. Aki (2003), Location of seismic events and eruptive  
 795 fissures on the Piton de la Fournaise volcano using seismic amplitudes, *J.*  
 796 *Geophys. Res.*, *108*(B8), doi:10.1029/2002JB002193.
- 797 Battaglia, J., V. Ferrazzini, T. Staudacher, K. Aki, and J. Cheminee (2005),  
 798 Pre-eruptive migration of earthquakes at the Piton de la Fournaise volcano

- 799 (Reunion Island), *Geophys. J. Int.*, *161*(2), 549–558.
- 800 Carmichael, I., J. Nicholls, F. Spera, B. Wood, and S. Nelson (1977), High-  
801 Temperature Properties of Silicate Liquids: Applications to the Equilibra-  
802 tion and Ascent of Basic Magma, *Phil. Trans. R Soc. Lond. A*, *286*(1336),  
803 373–429.
- 804 Cornet, F. (1992), Fracture processes induced by forced fluid percolation, in  
805 *Volcanic Seismology, IAVCEI Proc. Volcanology*, vol. 3, pp. 407–431.
- 806 Einarsson, P., and B. Brandsdottir (1980), Seismological evidence for lateral  
807 magma intrusion during the 1978 deflation of the Krafla volcano in NE  
808 Iceland, *J. Geophys.*, *47*, 160–165.
- 809 Froger, J., Y. Fukushima, P. Briole, T. Staudacher, T. Souriot, and N. Vil-  
810 leneuve (2004), The deformation field of the August 2003 eruption at Piton  
811 de la Fournaise, Reunion Island, mapped by ASAR interferometry, *Geo-*  
812 *phys. Res. Lett.*, *31*(14), L14,601.
- 813 Grasso, J., and P. Bachelery (1995), Hierarchical organization as a diagnostic  
814 approach to volcano mechanics: Validation on Piton de la Fournaise, *J.*  
815 *Geophys. Res.*, *22*, 2897–2900.
- 816 Ida, Y. (1999), Effects of the crustal stress on the growth of dikes: Conditions  
817 of intrusion and extrusion of magma , *J. Geophys. Res.*, *104*(B8), 17897–  
818 17909.
- 819 Klein, F., R. Koyanagi, J. Nakata, and W. Tanigawa (1987), The seismicity  
820 of Kilauea’s magma system, *Volcanism in Hawaii*, *2*, 1019–1185.

- 821 Lahaie, F., and J. Grasso (1998), A fluid-rock interaction cellular automa-  
822 tion of volcano mechanics: Application to the Piton de la Fournaise, *J.*  
823 *Geophys. Res.*, *103*, 9637–9649.
- 824 Lénat, J., and P. Bachèlery (1990), Structure et fonctionnement de la zone  
825 centrale du Piton de la Fournaise, in *Le Volcanisme de La Réunion*,  
826 edited by J. Lénat, pp. 257–296, Centre de Recherches Volcanologiques,  
827 Clermont-Ferrand, France.
- 828 Lister, J. (1990a), Buoyancy-driven fluid fracture: the effects of material  
829 toughness and of highly viscous fluids, *J. Fluid Mech.*, *210*, 263–280.
- 830 Lister, J. (1990b), Buoyancy-driven fluid fracture: similarity solutions for the  
831 horizontal and vertical propagation of fluid-filled cracks, *J. Fluid Mech.*,  
832 *217*, 213–239.
- 833 Lister, J., and R. Kerr (1991), Fluid-mechanical models of crack propaga-  
834 tion and their application to magma transport in dykes, *J. Geophys. Res.*,  
835 *96*(B6), 10049–10077.
- 836 Maaløe, S. (1998), Shape of ascending feeder dikes, and ascent modes of  
837 magma, *J. of Volcanol. Geotherm. Res.*, *81*(3-4), 207–214.
- 838 McKenzie, D. (1984), The Generation and Compaction of Partially Molten  
839 Rock, *J. Petrology*, *25*(3), 713–765.
- 840 Meriaux, C., and C. Jaupart (1998), Dike propagation through an elastic  
841 plate, *J. Geophys. Res.*, *103*, 18–18.
- 842 Mériaux, C., J. Lister, V. Lyakhovskiy, and A. Agnon (1999), Dyke propa-  
843 gation with distributed damage of the host rock, *Earth Planet. Sci. Lett.*,

844 165(2), 177–185.

845 Muskhelishvili, N. (1963), *Some Basic Problems of the Mathematical Theory*  
846 *of Elasticity: Fundametal Equations, Plane Theory of Elasticity, Torsion*  
847 *and Bending*, Noordhoff.

848 Nercessian, A., A. Hirn, J. Lépine, and M. Sapin (1996), Internal struc-  
849 ture of Piton de la Fournaise volcano from seismic wave propagation and  
850 earthquake distribution, *J. Volcanol. Geother. Res.*, 70(3-4), 123–143.

851 Nishimura, T., S. Ozawa, M. Murakami, T. Sagiya, T. Tada, M. Kaidzu, and  
852 M. Ukawa (2001), Crustal deformation caused by magma migration in the  
853 northern Izu Islands, Japan, *Geophys. Res. Lett.*, 28(19), 3745–3748.

854 Pasteris, J. (1984), Kimberlites: Complex Mantle Melts, *Annu. Rev. Earth*  
855 *Planet. Sci.*, 12(1), 133–153.

856 Pedersen, R., F. Sigmundsson, and P. Einarsson (2007), Controlling factors  
857 on earthquake swarms associated with magmatic intrusions; Constraints  
858 from Iceland, *J. Volcanol. Geotherm. Res.*, 162(1-2), 73–80.

859 Peltier, A., V. Ferrazzini, T. Staudacher, and P. Bachèlery (2005), Imaging  
860 the dynamics of dyke propagation prior to the 2000–2003 flank eruptions at  
861 Piton de La Fournaise, Reunion Island, *Geophys. Res. Lett.*, 32, L22,302.

862 Peltier, A., T. Staudacher, and P. Bachèlery (2007), Constraints on  
863 magma transfers and structures involved in the 2003 activity at Piton  
864 de La Fournaise from displacement data, *J. Geophys. Res.*, 112(B03207),  
865 doi:10.1029/2006JB0004379.

- 866 Peltier, A., V. Famin, P. Bachčlery, V. Cayol, Y. Fukushima, and T. Stau-  
867 dacher (2008), Cyclic magma storages and transfers at Piton de La Four-  
868 naise volcano (La Réunion hotspot) inferred from deformation and geo-  
869 chemical data, *Earth Planet. Sci. Lett.*, *270*, 180–188.
- 870 Peltier, A., P. Bachèlery, and T. Staudacher (2009), Magma transport and  
871 storage at Piton de La Fournaise (La Réunion) between 1972 and 2007:  
872 A review of geophysical and geochemical data, *J. Volcanol. Geother. Res.*,  
873 *184*, 93–108.
- 874 Pinel, V., and C. Jaupart (2000), The effect of edifice load on magma ascent  
875 beneath a volcano, *Phil. Trans. R. Soc. A*, *358*(1770), 1515–1532.
- 876 Pinel, V., and C. Jaupart (2004), Magma storage and horizontal dyke injec-  
877 tion beneath a volcanic edifice, *Earth Planet. Sci. Lett.*, *221*(1-4), 245–262.
- 878 Pitcher, W. (1979), The nature, ascent and emplacement of granitic magmas,  
879 *J. Geol. Soc.*, *136*(6), 627–662.
- 880 Prôno, E., J. Battaglia, V. Monteiller, J. Got, and V. Ferrazzini (2009),  
881 P-wave velocity structure of Piton de la Fournaise volcano deduced from  
882 seismic data recorded between 1996 and 1999, *J. Volcanol. Geotherm. Res.*,  
883 *184*(1-2), 49–62.
- 884 Roper, S., and J. Lister (2005), Buoyancy-driven crack propagation from an  
885 over-pressured source., *J. Fluid Mech.*, *536*, 79–98.
- 886 Rubin, A. (1993a), Dikes vs. diapirs in viscoelastic rock, *Earth Planet. Sci.*  
887 *Lett.*, *119*(4), 641–659.

- 888 Rubin, A. (1993b), Tensile fracture of rock at high confining pressure: impli-  
889 cations for dyke propagation, *J. Geophys. Res.*, *98*(B 9), 15,919–15,935.
- 890 Rubin, A. (1995), Propagation of Magma-Filled Cracks, *Annu. Rev. Earth*  
891 *Planet. Sci.*, *23*(1), 287–336.
- 892 Rubin, A., and D. Gillard (1998), Dike-induced earthquakes: Theoretical  
893 considerations, *J. Geophys. Res.*, *103*(B5), 10,017–10,030.
- 894 Rubin, A., D. Gillard, and J. Got (1998), A reinterpretation of seismicity as-  
895 sociated with the January 1983 dike intrusion at Kilauea Volcano, Hawaii,  
896 *J. Geophys. Res.*, *103*(B5), 10,003–10,015.
- 897 Sapin, M., A. Hirn, J. L epine, and A. Nercessian (1996), Stress, failure and  
898 fluid flow deduced from earthquakes accompanying eruptions at Piton de  
899 la Fournaise volcano, *J. Volcanol. Geotherm. Res.*, *70*(3-4), 145–167.
- 900 Shaw, H. (1980), The fracture mechanisms of magma transport from the  
901 mantle to the surface, *Phys. Magmat. Proc.*, 201–264.
- 902 Sigmarsson, O., M. Condomines, and P. Bach elery (2005), Magma residence  
903 time beneath the Piton de la Fournaise Volcano, Reunion Island, from  
904 U-series disequilibria, *Earth Planet. Sci. Lett.*, *234*(1-2), 223–234.
- 905 Spera, F. (1980), Aspects of magma transport, *Phys. Magmat. Proc.*, 265–  
906 323.
- 907 Taisne, B., and C. Jaupart (in press, 2009), Dyke Propagation Through  
908 Layered Rocks, *J. Geophys. Res.*
- 909 Tinard, P. (2007), Caract erisation et mod elisation des d placements du sol  
910 associ es a l’activit e volcanique du Piton de la Fournaise, ile de la R union,

- 911 a partir de données interférométriques. Aout 2003 - Avril 2007, Ph.D. thesis,  
912 Université Blaise Pascal - Clermont-Ferrand II.
- 913 Toda, S., R. Stein, and T. Sagiya (2002), Evidence from the AD 2000 Izu  
914 islands earthquake swarm that stressing rate governs seismicity, *Nature*,  
915 *419*, 58–61.
- 916 Toutain, J., P. Bachelery, P. Blum, J. Cheminee, H. Delorme, L. Fontaine,  
917 P. Kowalski, and P. Taochy (1992), Real time monitoring of vertical ground  
918 deformations during eruptions at Piton de la Fournaise, *Geophys. Res. Lett.*,  
919 *19*(6), 553–556.
- 920 Traversa, P., and J. Grasso (2009), Brittle Creep Damage as the Seismic  
921 Signature of Dyke Propagations within Basaltic Volcanoes, *Bull. Seismol.*  
922 *Soc. America*, *99*(3), 2035-2043.
- 923 Villeneuve, N., D. Neuville, P. Boivin, P. Bachelery, and P. Richet (2008),  
924 Magma crystallization and viscosity: A study of molten basalts from the  
925 Piton de la Fournaise volcano (La Réunion island), *Chemical Geology*,  
926 *256*(3-4), 241–250.



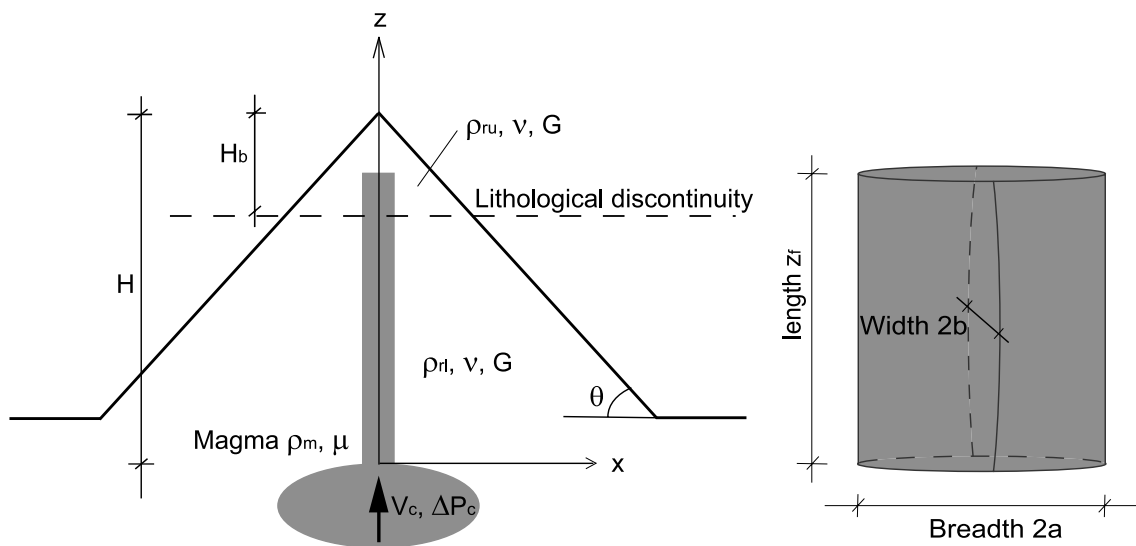


**Figure 1.** Sketch illustrating the geometry of a vertical dyke (left) and the shape of the fissure (right).  $2b \ll 2a \leq z_f$ . Half breadth  $a$  is assumed a priori.

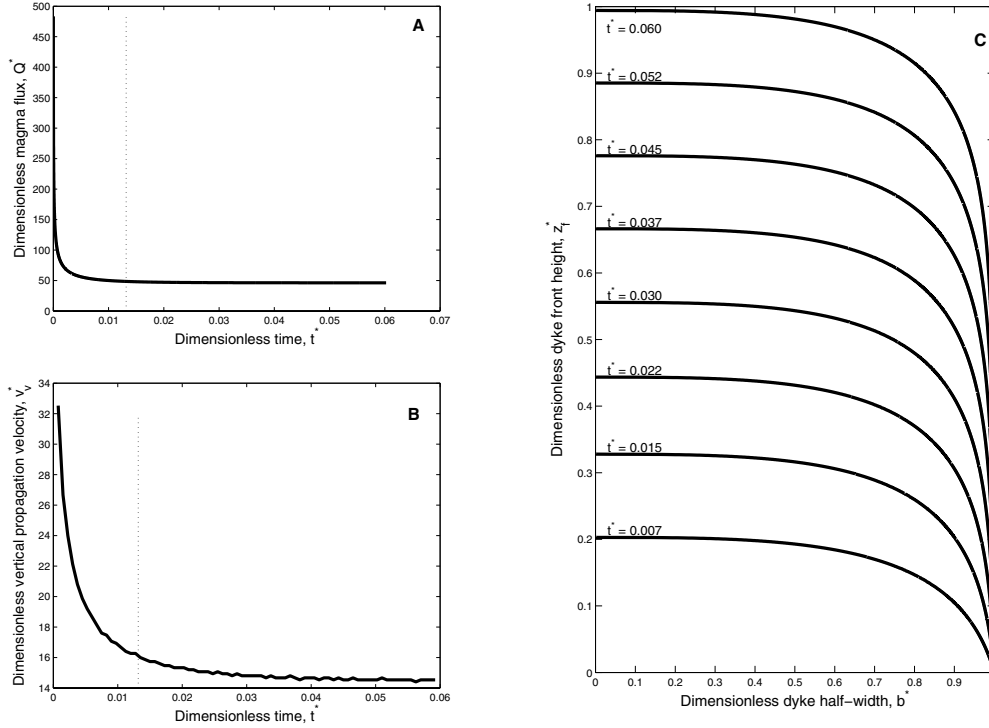


**Figure 2.** Magma-filled dyke rising in a homogeneous medium from a constant overpressure magma chamber at depth. A: dimensionless magma flux injected into the dyke over time; B: dimensionless propagation velocity versus time; C: Evolution of the crack shape for progressive growth stages.  $R_1$  ( $R_1 = (\rho_m - \rho_r)gH/\Delta P_0$ ) value used in the calculation is -3.55. Stipple-lines in plots A and B indicate  $z_f^* = 0.3$ . Reminder:  $t = t^*[t]$ ,  $Q = Q^*[Q]$ ,  $v_v = v_v^*[v]$ ,  $b = b^*[b]$ ,  $z_f = z_f^*[H]$ , where scales for time  $[t]$ , flux  $[Q]$  and fracture width  $[b]$  are given in equations (6) to (8), lengths are scaled by the reservoir depth  $H$ , and scale for propagation velocity is  $[v] = [H]/[t]$ .

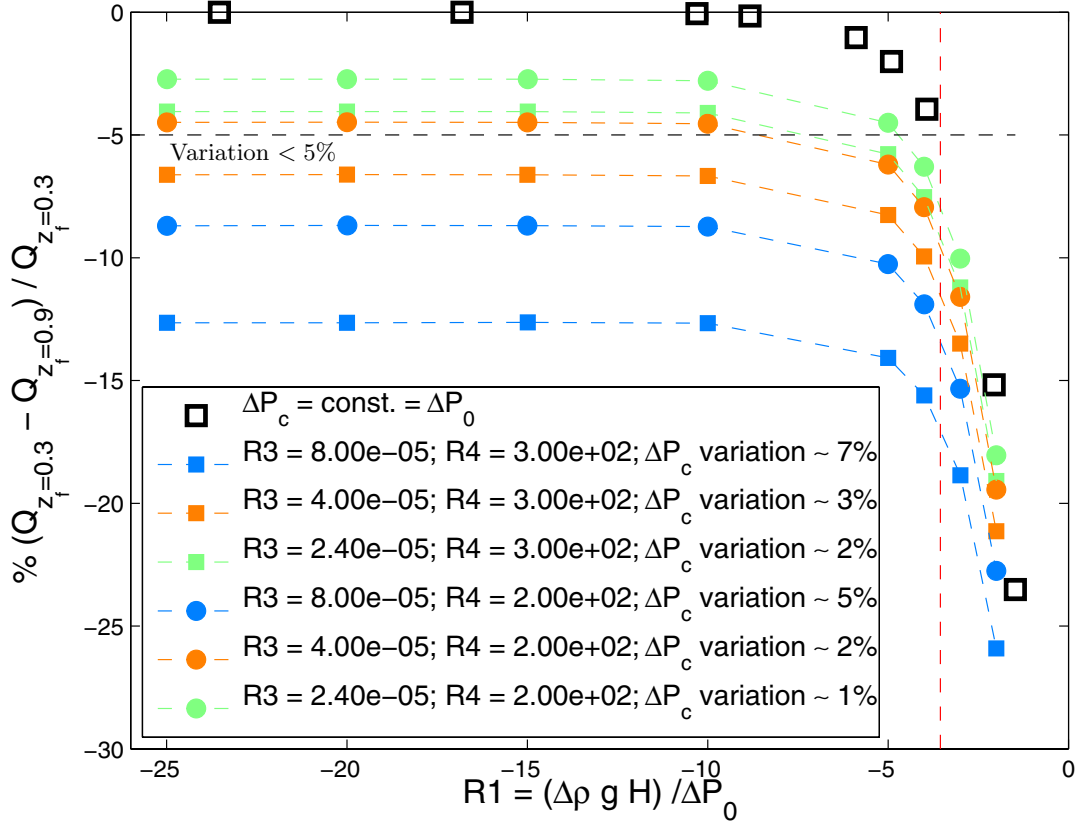


**Figure 3.** Percentage of magma influx variation during dyke growth within a homogeneous medium as function of the dimensionless number  $R_1$  ( $R_1 = (\rho_m - \rho_r)gH/\Delta P_0$ ). Black squares: constant overpressure at the dyke inlet; colored symbols: variable overpressure in the chamber. Color of solid symbols is related to the  $V_c$  value; circles or square symbols depend on the  $K$  value. Reservoir overpressure variations  $\Delta P_c$  variation indicated in the legend are issued from the computation.

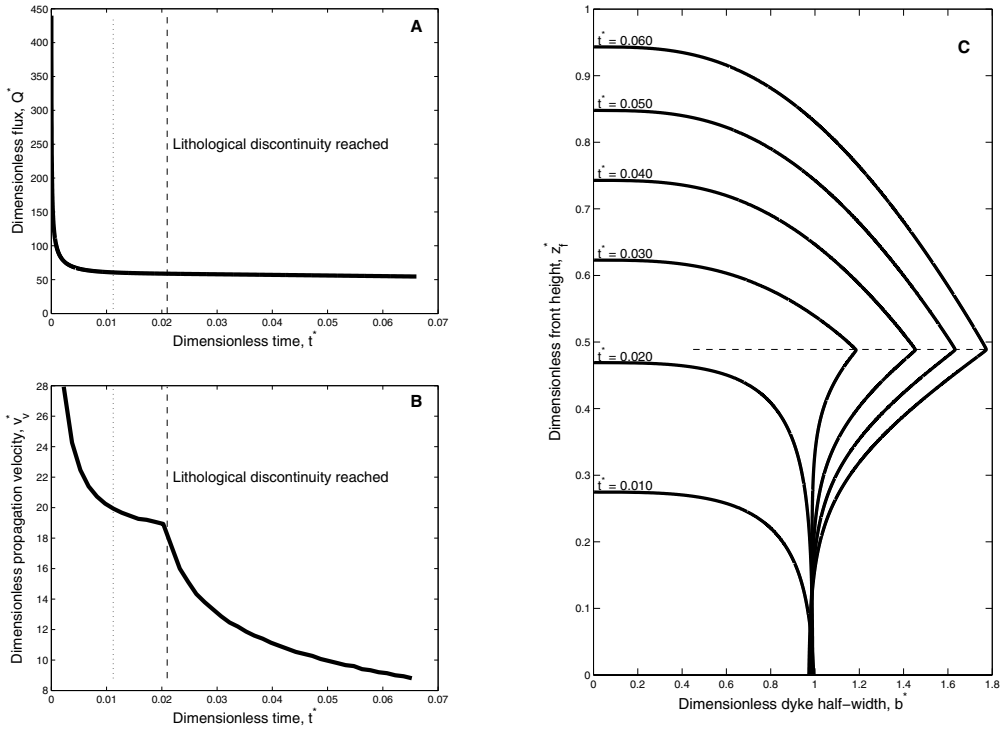


**Figure 4.** Magma-filled dyke rising in a homogeneous medium from a constant overpressure magma chamber at depth. A: dimensionless magma flux injected into the dyke over time; B: dimensionless propagation velocity versus time; C: Evolution of the crack shape for progressive growth stages. Parameter values used in the computation are:  $R_{1l} = -4.82$ ,  $R_{1u} = 1.37$ ,  $R_2 = 0.51$ ,  $R_3 = 6.9 \times 10^{-9}$ ,  $R_4 = 1.125$ . Stipple-lines in plots A and B indicate  $z_f^* = 0.3$ . Reminder:  $t = t^*[t]$ ,  $Q = Q^*[Q]$ ,  $v_v = v_v^*[v]$ ,  $b = b^*[b]$ ,  $z_f = z_f^*[H]$ , where scales for time  $[t]$ , flux  $[Q]$  and fracture width  $[b]$  are given in equations (6) to (8), lengths are scaled by the reservoir depth  $H$ , and scale for propagation velocity is  $[v] = [H]/[t]$ ;  $R_{1u} = (\rho_m - \rho_{ru})gH/\Delta P_0$ ,  $R_{1l} = (\rho_m - \rho_{rl})gH/\Delta P_0$ ,  $R_2 = H_b/H$ ,  $R_3 = (\Delta P_0 a^2 (1 - \nu) H) (G V_c)$ ,  $R_4 = 4KG/(\Delta P_0 (4G + 3K))$ .

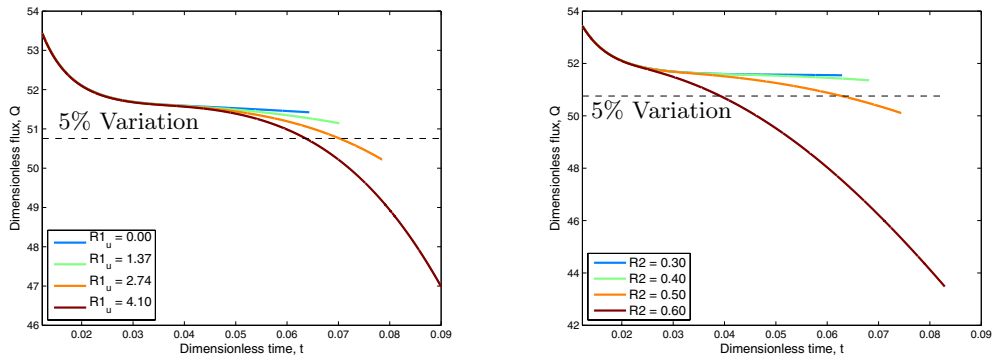


**Figure 5.** Left: effect of the dimensionless number  $R_{1ru}$  on the magma flux evolution over time during dyke propagation,  $R_2 = 0.43$ . Right: effect of the dimensionless number  $R_2$  on the magma flux evolution over time during dyke propagation,  $R_{1ru} = 1.37$ . For both cases  $R_{1rl} = -4.1$ ,  $V_c = 5 \text{ km}^3$  and  $K = 1 \times 10^9 \text{ Pa}$ . Final time corresponds to surface attainment. **Reminder:**  $R_{1u} = (\rho_m - \rho_{ru})gH/\Delta P_0$ ,  $R_{1l} = (\rho_m - \rho_{rl})gH/\Delta P_0$ ,  $R_2 = H_b/H$ ,  $R_3 = (\Delta P_0 a^2 (1-\nu) H) (G V_c)$ ,  $R_4 = 4KG/(\Delta P_0 (4G + 3K))$ .

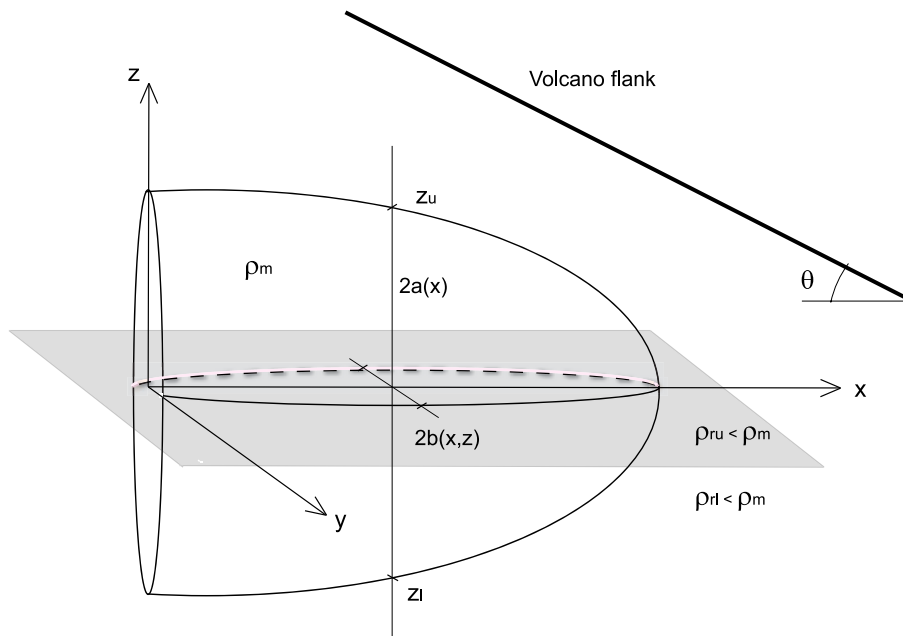


**Figure 6.** Sketch illustrating the geometry and the main parameters of a dyke horizontally propagating at the Level of Neutral Buoyancy

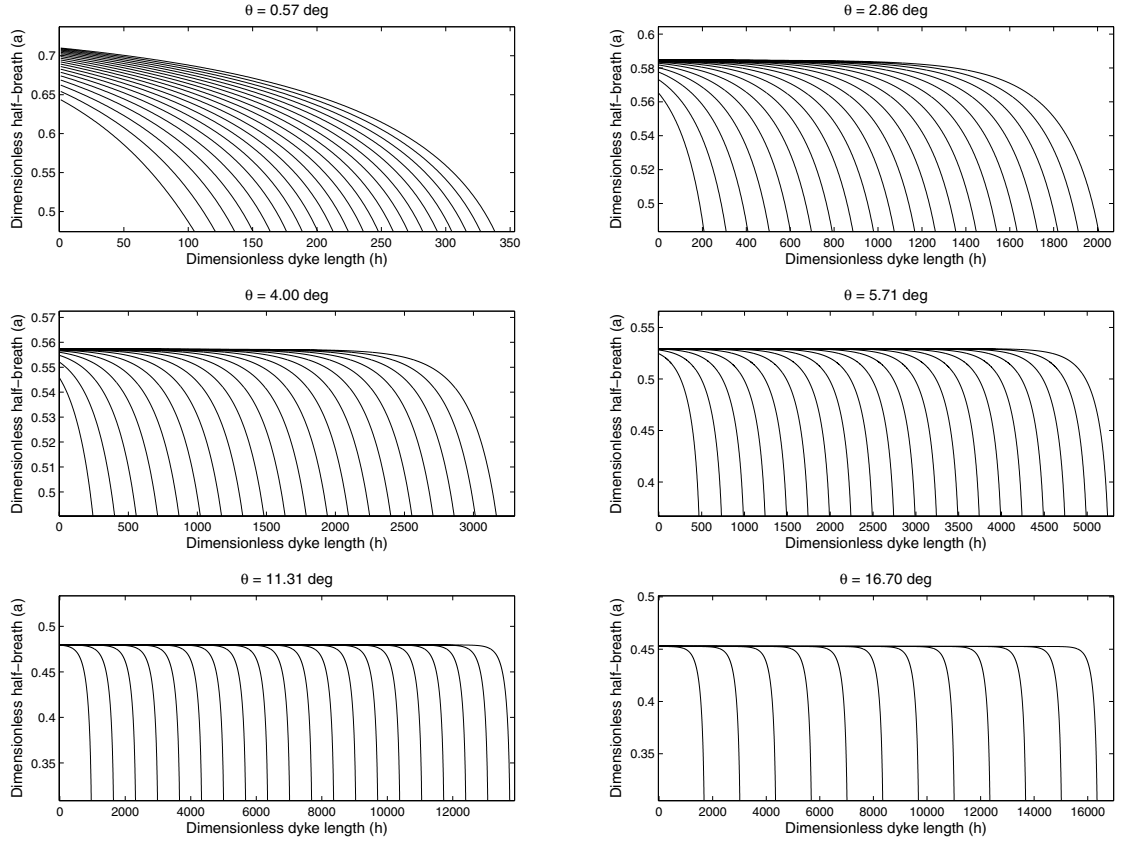


**Figure 7.** Lateral dyke propagation: effect of the edifice flank slope on the fracture shape evolution over time. Parameters used in the calculations are:  $\rho_{rl} = 2700 \text{ kg m}^{-3}$ ,  $\rho_{ru} = 2300 \text{ kg m}^{-3}$ ,  $\rho_m = 2400 \text{ kg m}^{-3}$ . Dimensionless time step between following curves is  $10^{-6}$ . Dimensionless numbers values are:  $N_1 = 1.65 \times 10^{-4}$  and  $N_2 = -1.48 \times 10^8$ . **Reminder:**  $N_1 = (3Q_{in}^{3/4} \mu^{3/4} G^{9/4}) / (H_b^{9/4} (1 - \nu)^{9/4} [P]^3)$ ,  $N_2 = -(2H_b^3 (1 - \nu)^3 [P]^4) / (3\mu Q_{in} G^3)$ .

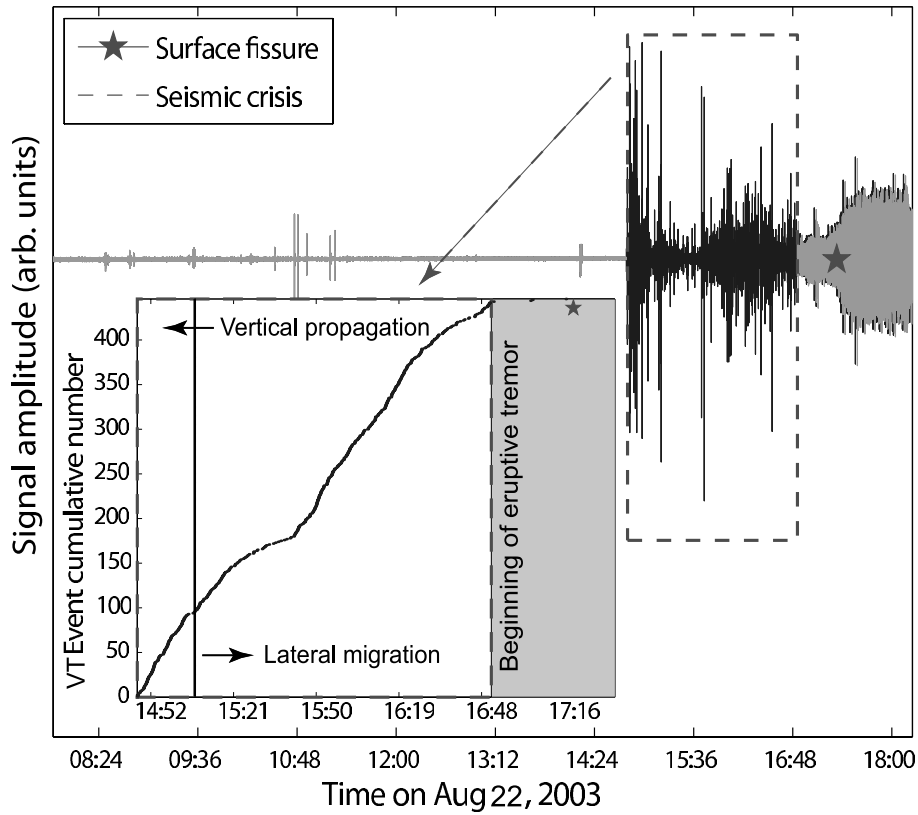


**Figure 8.** Seismic signal and cumulated seismicity (inset) hand-picked from continuous recordings recorded at the BOR summit station during the August 22 2003 dyke intrusion at Piton de la Fournaise volcano. Times related to the different stages of activity are from *Peltier et al.* [2007].



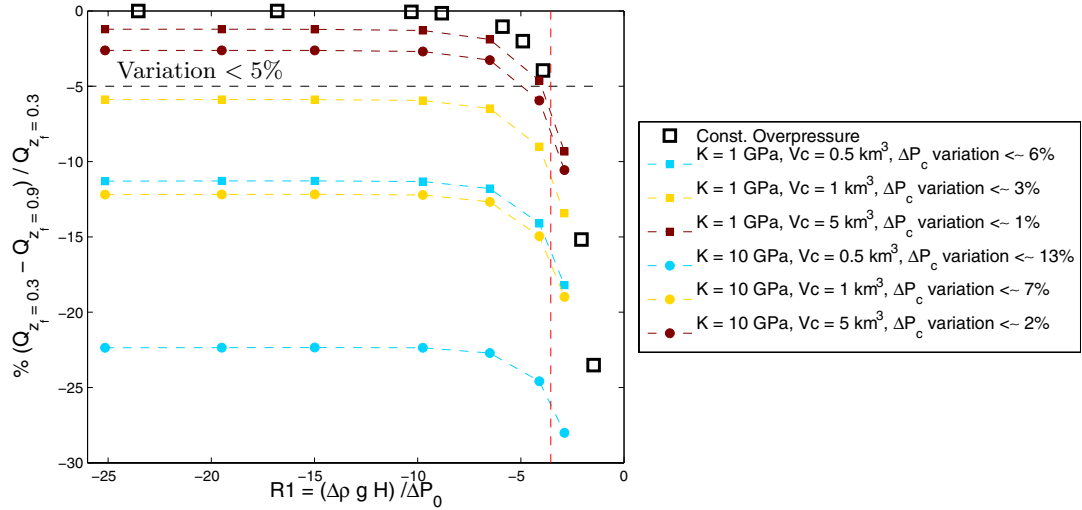


**Figure 9.** Interrelationship between magma influx and reservoir characteristics. Percentage of magma influx variation during dyke growth within a homogeneous medium as function of the dimensionless number  $R_1$  ( $R_1 = (\rho_m - \rho_r)gH/\Delta P_0$ ). Black squares: constant overpressure at the dyke inlet; colored symbols: variable overpressure in the chamber. Colors of plain symbols are related to the  $V_c$  value; circles or square symbols depend on the  $K$  value. Reservoir overpressure variations  $\Delta P_c$  variation indicated in the legend are issued from the computation. Parameter values used are:  $G = 1.125 \times 10^9$  Pa,  $\nu = 0.25$ ,  $a = 100$  m,  $g = 9.81$  m s $^{-2}$ .  $V_c$  values derive from conceptual models of PdfF storage system [Nercessian *et al.*, 1996; Sapin *et al.*, 1996; Peltier *et al.*, 2007, 2008].

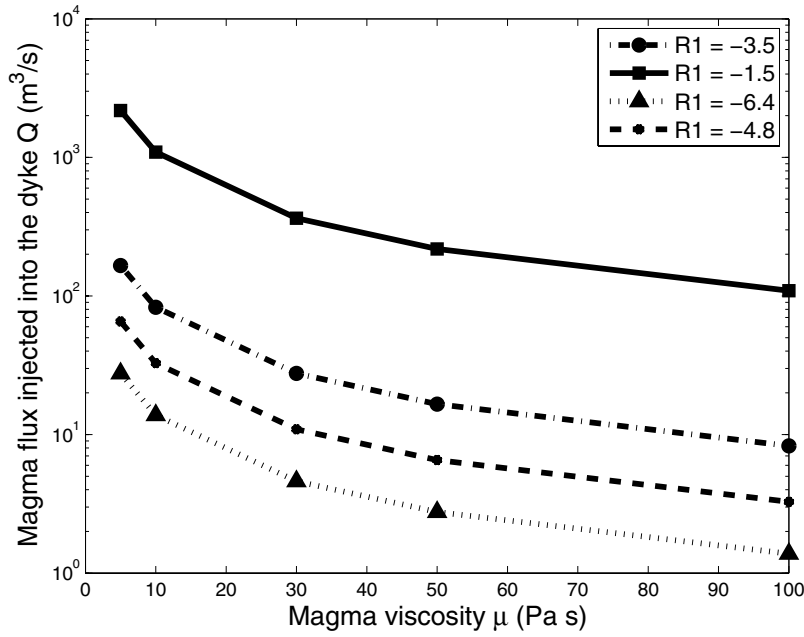


**Figure 10.** Dyke rising vertically within a homogeneous medium from a constant overpressure magma reservoir. Magma flux injected into the dyke as function of the magma viscosity and of the dimensionless number  $R_1$  ( $R_1 = (\rho_m - \rho_r)gH/\Delta P_0$ ). Parameters used are:  $H = 2250$  m,  $\rho_m = 2400$  kg m<sup>-3</sup>,  $\rho_r = 2750$  kg m<sup>-3</sup>,  $a = 100$  m,  $\nu = 0.25$ ,  $G = 1.125 \times 10^9$  Pa.

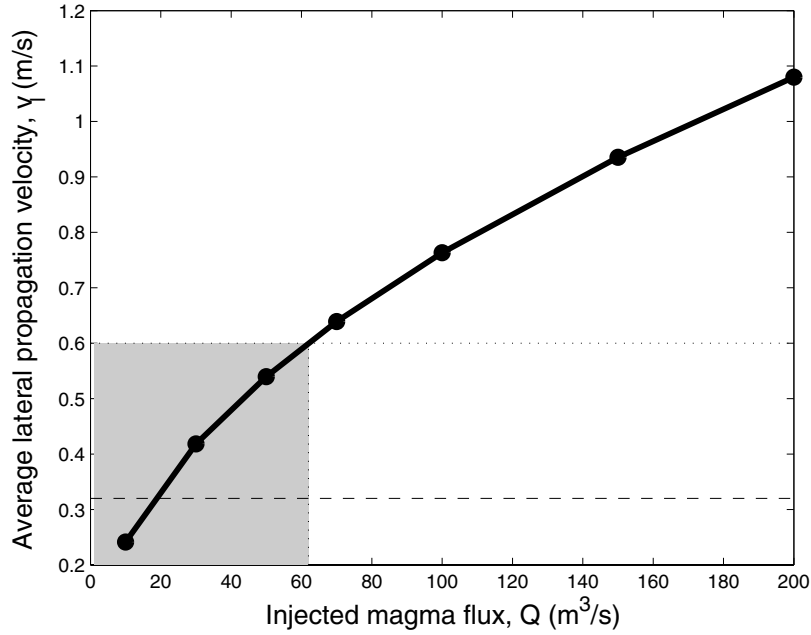


**Figure 11.** Lateral dyke propagation: average propagation velocity versus influx of magma injected into the dyke. Shaded area bounds the lateral propagation velocities estimated by *Peltier et al.* [2007] at Piton de la Fournaise. Parameters used are the following:  $\theta = 11.8$  deg,  $\rho_{rl} = 2750$  kg m $^{-3}$ ,  $\rho_{ru} = 2300$  kg m $^{-3}$ ,  $\rho_m = 2400$  kg m $^{-3}$ ,  $H_b = 1150$  m,  $G = 1.125 \times 10^9$  Pa. Each magma flux value corresponds to a viscosity value, according to equation 39, where  $A = 4.3936$  (from the vertical homogeneous case  $R_1 = -3.55$ ). **Reminder:**  $R_1 = (\rho_m - \rho_r)gH/\Delta P_0$ .

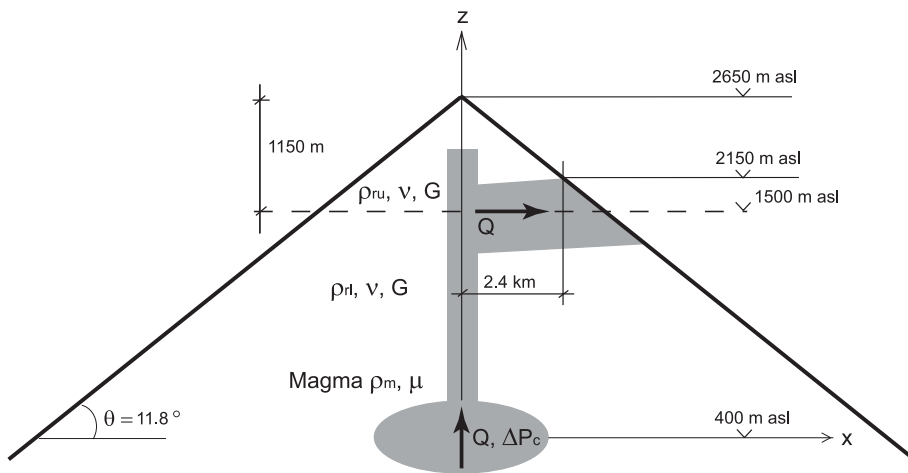


**Figure 12.** August 2003 PdIF case study. Sketch illustrating the geometry used in the model. Dotted line: input lithological discontinuity, position from *Peltier et al.* [2007]. Gray zones indicate magma path. All elevation data come from *Peltier et al.* [2007].

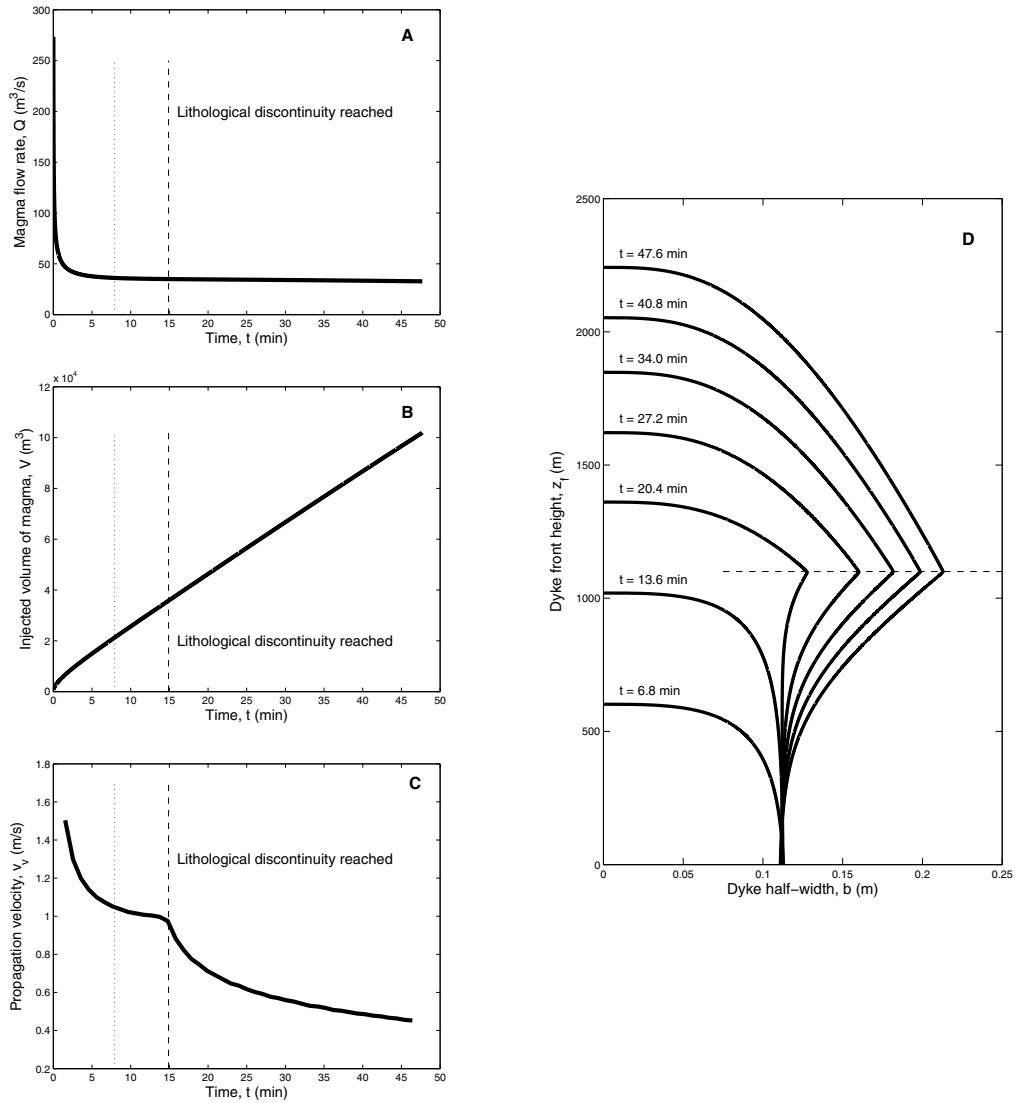


**Figure 13.** The effect of a lithological discontinuity on the vertical propagation of a magma-filled dyke. A: magma flux injected into the dyke over time; B: dyke volume (i.e. cumulative volume of magma injected into the dyke over time); C: propagation velocity versus time; D: Evolution of the crack shape for progressive growth stages. Parameter values used in the calculation are listed in table 2. Stippled lines in plots A, B and C correspond to  $z_f/H = z_f^* = 0.3$ .

**Table 1.** Parameters used in the calculations for the case of a dyke rising in a homogenous medium from a large and fully compressible magma reservoir. †: from *Peltier et al.* [2007]; ‡: assumed parameters, as generic basalt values.

Parameter	Symbol	Value
Depth of the reservoir (m)†	$H$	2250
Poisson's ratio‡	$\nu$	0.25
Shear modulus (Pa)‡	$G$	$1.125 \times 10^9$
Rock density ( $\text{kg m}^{-3}$ )‡	$\rho_r$	2750
Magma density ( $\text{kg m}^{-3}$ )‡	$\rho_m$	2400

**Table 2.** Parameters used in the calculations applied to the August 2003 eruption at Piton de la Fournaise. †: parameter values estimated by *Peltier et al.* [2007]; ‡: assumed parameters as generic basalt values; § derived parameters; ⊗ parameter values from literature [e.g. *Lénat and Bachèlery*, 1990; *Nercessian et al.*, 1996; *Sapin et al.*, 1996; *Pinel and Jaupart*, 2000, 2004; *Peltier et al.*, 2008].

Parameter	Symbol	Value
Depth of the reservoir(m)†	$H$	2250
Half-length of the fracture(m)§	$a$	100
Poisson's ratio‡	$\nu$	0.25
Shear modulus (Pa)‡	$G$	$1.125 \times 10^9$
Rock density in the upper layer ( $\text{kg m}^{-3}$ )‡	$\rho_{ru}$	2300
Rock density in the lower layer ( $\text{kg m}^{-3}$ )‡	$\rho_{rl}$	2750
Depth of the lithological discontinuity (m)†	$H_b$	1150
Density of magma ( $\text{kg m}^{-3}$ )‡	$\rho_m$	2400
Magma viscosity ( $\text{Pa s}$ )§	$\mu$	11
Initial magma chamber overpressure (MPa)§:	$\Delta P_0$	1.7
Edifice slope (deg)§	$\theta$	11.8
Magma chamber volume ( $\text{km}^3$ )⊗	$V_c$	1.7
Magma bulk modulus (Pa)‡	$K$	$1 \times 10^9$
Dimensionless numbers		
$R_{1l} = (\rho_m - \rho_{rl})gH/\Delta P_0$	$R_{1l}$	-4.54
$R_{1u} = (\rho_m - \rho_{ru})gH/\Delta P_0$	$R_{1u}$	1.30
$R_2 = H_b/H$	$R_2$	0.51
$R_3 = (\Delta P_0 a^2 (1 - \nu) H) (G V_c)$	$R_3$	$1.5 \times 10^{-5}$
$R_4 = 4KG/(\Delta P_0 (4G + 3K))$	$R_4$	352.90

**Table 3.** Model validation on the August 2003 Piton de la Fournaise eruption. Comparison between independent parameter estimations based on deformation data (from *Peltier et al.* [2007]) and computation results. \*: [Peltier 2009, personal communication].

Parameter	Observation estimate	Model output
Vertical average dyke propagation velocity ( $\text{m s}^{-1}$ )	$1.3 \pm 0.26^*$	1.23
Lateral average dyke propagation velocity ( $\text{m s}^{-1}$ )	$0.2 - 0.6 \pm 0.13^*$	0.48
Lateral phase duration (min)	125	81
Lateral covered distance (m)	$2400 \pm 100^*$	2300
Dyke total volume ( $\text{m}^3$ )	$1 \pm 0.23^* \times 10^6$	$0.82 \times 10^6$